IJEAS

International Journal of Engineering & Applied Sciences

IJEAS

Abstracting & Indexing

Editorial Scope

The journal presents its readers with broad coverage across some branches of engineering and science of the latest development and application of new solution algorithms, artificial intelligent techniques innovative numerical methods and/or solution techniques directed at the utilization of computational methods in solid and nano-scaled mechanics.

International Journal of Engineering & Applied Sciences (IJEAS) is an Open Access Journal

International Journal of Engineering & Applied Sciences (IJEAS) publish original contributions on the following topics:

Civil Engineering: numerical modelling of structures, seismic evaluation, experimental testing, construction and management, geotechnical engineering, water resources management, groundwater modelling, coastal zone modelling, offshore structures, water processes, desalination, waste-water treatment, pavement and maintenance, transport and traffic, laser scanning, and hydrographic surveying, numerical methods in solid mechanics, nanomechanic and applications, microelectromechanical systems (MEMS), vibration problems in engineering, higher order elasticity (strain gradient, couple stress, surface elasticity, nonlocal elasticity)

Electrical Engineering: artificial and machine intelligence and robotics, automatic control, bioinformatics and biomedical engineering, communications, computer engineering and networks, systems security and data encryption, electric power engineering and drives, embedded systems, Internet of Things (IoT), microwaves and optics.

Engineering Mathematics and Physics: computational and stochastic methods, optimization, nonlinear dynamics, modelling and simulation, computer science, solid state physics and electronics, computational electromagnetics, biophysics, atomic and molecular physics, thermodynamics, geophysical fluid dynamics, wave mechanics, and solid mechanics.

Mechanical Engineering: machine design, materials science, mechanics of materials, manufacturing engineering and technology, dynamics, robotics, control, industrial engineering, ergonomics, energy, combustion, heat transfer, fluids mechanics, thermodynamics, turbo machinery, aerospace research, aerodynamics, and propulsion.

CONTENTS

A Finite Element Solution for Bending Analysis of a Nanoframe using Modified Couple Stress Theory

*Büşra Uzun *, M. Özgür Yaylı*

Bursa Uludag University, Engineering Faculty, Department of Civil Engineering
Division of Mechanics, Bursa-TURKEY
**E-mail address*: buzun@uludag.edu.tr *, ozguryayli@uludag.edu.tr*

ORCID numbers of authors:
*0000-0002-7636-7170 *, 0000-0003-2231-170X*

Abstract

In this work, a finite element formulation for a size dependent frame system is presented. Size dependency is discussed via the modified couple stress theory. The nodal displacement and rotation analyses of a frame system with total of three elements, including two columns and one beam element connecting these two columns, are considered. The classical stiffness and size dependent stiffness matrices of frame system are derived. Then, solution procedure for this problem is explained. Lastly, a numerical application is realized and effect of material length scale parameter on nodal displacements and rotations is discussed. To present the numerical application, it is assumed that the elements of the nanoframe are composed of silicon carbide nanotubes.

Keywords: Modified couple stress theory, Frame system, Static, Finite element method

1. Introduction

Nanotechnology covers the manufacture and understanding of the nanoscale materials /elements / systems. Nanotechnology controls materials and devices at atomic and molecular levels, enabling them to be arranged or reconstructed. The properties of enormously small materials, which are much better than expected, have attracted great interest. Thus, studies on the discovery of new nanomaterials and the understanding of the properties of discovered nanomaterials have begun to increase. Especially, carbon nanotubes [1] have attracted much attention and many studies have been carried out on the usage areas and synthesis methods of such nanomaterials. These studies have accelerated and the synthesis of various nanomaterials and nanostructures has begun. Recently, it has been seen that studies [2-4] on more complicated nanostructures (nanoframes) have been presented. In these studies, various properties such as the architecture, oxygen reaction reduction activity, the exciton decay time, and catalytic performance of various nanoframe structures were discussed.

Studies have revealed that nanoscale materials are affected by some parameters and manipulations that do not affect conventional materials. In nanomaterials, parameters such as the changed length, the number of atoms that constitute them etc., can vary the behavior of

1

these material. This is called the size effect. The size effect is important for nanomaterials. Because in order to design correctly applications of nano-electromechanical systems/micro-electromechanical systems (NEMS/MEMS), it is important to know the behavior of the materials that constitute them. Continuum mechanics theories based on the size effect have an important place among the practical methods that contribute to the revealing of these behaviors. Some of these size dependent theories are: nonlocal elasticity theory, modified couple stress theory, modified strain gradient theory, doublet mechanics theory, nonlocal strain gradient theory, surface elasticity theory.

Structures such as rods, beams, plates, and frames have recently been modeled at nano and micro scales and their various analyzes like static, vibration and buckling have been carried out based on the mentioned size dependent theories. Navier's method [5-11], Fourier sine solution [12-17], finite element method [18-29], separation of variable procedure [30, 31], generalized differential quadrature method [32-36], Ritz method have been frequently used by scholars to present the mechanical responses of various small scale structures such as nanobeam, nanoframe, nanotruss, nanorod, nanoplate, cracked microbeam with functionally graded material, cracked nanobeam, functionally graded nanobeam, porous nanotube etc. The above-mentioned solution methods and others have been also utilized for macro-dimensional porous plate [37-39], porous beam [40, 41], beam [42], reinforced plate [43, 44], functionally graded and laminated beam [45-50], shell [51], functionally graded and laminated plate [52], functionally graded shell [53], reinforced beam [54], frame [55] structures.

In this study, the analyzes are carried out using the finite element method. The finite element method has attracted attention with its practical solution and applicability to a wide variety of problems. The finite element method, which is used for the analysis of macro-scale elements and structures, has recently been used frequently for the analysis of nano- and micro-scale elements and structures after the size dependent elasticity theories. As can be understood from the above-mentioned papers, structures such as beams, plates, rods, and frames have been modeled at nano and micro scales and their theoretical analyzes have been carried out. When we look at the literature, it is understood that there are very few studies presenting the size effect analyzes of frame systems. To the best of the authors knowledge, this work for the first time, discusses the effect of material length scale parameter on the nodal displacement and rotation of a nano-sized frame in the context of modified couple stress theory. In this study, a size-dependent finite element formulation based on the modified couple stress theory that calculates the nodal displacement and rotation values of a nanoscale frame system is presented.
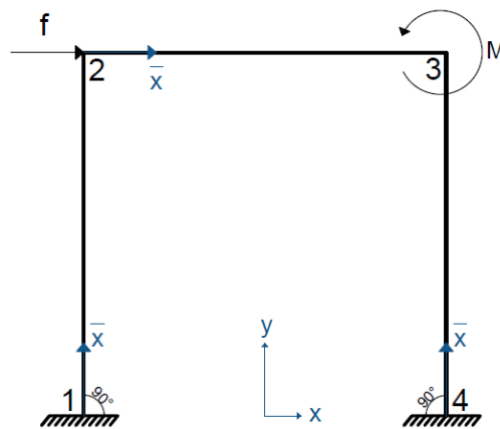
Fig.1. A nano-sized frame system

2. Modified Couple Stress Theory

Modified couple stress theory (MCST) is one of the higher-order elasticity theories used to perform size-based analyzes of nano- and micro-scale structures. For this theory proposed by Yang et al. [56], the strain energy U is expressed as follows:

$$U = \frac{1}{2}\int_V \left(\sigma_{ij}\varepsilon_{ij} + m_{ij}\chi_{ij}\right)dV \tag{1}$$

In the strain energy equation, σ_{ij}, ε_{ij} m_{ij} and χ_{ij} represent the the classical stress tensor, strain tensor, the symmetric couple stress tensor and symmetric rotation gradient tensor, respectively. Also, V denotes the volume occupied by body. After some mathematical procedures, the strain energy can be written as follows.

$$U = \frac{1}{2}\int_0^L \left(EA\left(\frac{\partial u}{\partial x}\right)^2 + \left(EI + GAl^2\right)\left(\frac{\partial^2 w}{\partial x^2}\right)^2 \right)dx \tag{2}$$

In which, L, I, A denote the length, moment of inertiea and cross-sectional areas, respectively. While E represents the Young's modulus, G denotes the shear modulus. u and w represent axial and transverse displacement fields, respectively. Lastly, l specifies the material length scale parameter. Material length scale parameter is a small size parameter. Thanks to this parameter, the analysis can be realised based on the size effect. Neglecting this parameter in the equations reduces the problem to classical theory and the problem becomes independent of the small size effect.

3. Finite Element Formulation Based on MCST for a Nanoframe System

The finite element solution, which allows us to find nodal displacements and rotations, is expressed as follows [57]:

$$\{F\} = [K]\{\bar{d}\} \tag{3}$$

In the above equation, {F}, [K] and {$\bar{d}$} specify the global nodal force vector, stiffness matrix and global nodal displacement vector, respectively. Interpolation functions are used to derived the stiffness matrix of the elements that constitute the frame system. These interpolation functions for the axial and transverse displacements are as follows [20, 22, 57]:

$$\psi^u = \begin{bmatrix} \psi_1^u \\ \psi_2^u \end{bmatrix} \tag{4}$$

In which,

$$\psi_1^u = 1 - \frac{x}{L_e}$$

$$\psi_2^u = \frac{x}{L_e}$$

(5)

Ψ^u is defined as interpolation functions for axial displacement. In addition to the axial displacement, interpolation functions for transverse displacement should be defined. The shape functions of transverse displacement indicated by Ψ^w are given as follows [22, 57]

$$\psi^w = \begin{bmatrix} \psi_1^w \\ \psi_2^w \\ \psi_3^w \\ \psi_4^w \end{bmatrix}$$

(6)

Here,

$$\psi_1^w = 1 - \frac{3x^2}{L_e^2} + \frac{2x^3}{L_e^3},$$

$$\psi_2^w = x - \frac{2x^2}{L_e} + \frac{x^3}{L_e^2}$$

$$\psi_3^w = \frac{3x^2}{L_e^2} - \frac{2x^3}{L_e^3},$$

$$\psi_4^w = -\frac{x^2}{L_e} + \frac{x^3}{L_e^2}$$

(7)

In the above equations, L_e represent the length of a finite element. Stiffness matrices are written via the obtained strain energy expression and interpolation functions given previous equations:

$$K_u = \int_0^{L_e} EA \left(\frac{\partial [\psi^u]}{\partial x} \right)^T \frac{\partial [\psi^u]}{\partial x} dx = EA \begin{bmatrix} \dfrac{1}{L_e} & \dfrac{-1}{L_e} \\ \dfrac{-1}{L_e} & \dfrac{1}{L_e} \end{bmatrix}$$

(8)

$$K_w = \int_0^{L_e} EI \left(\frac{\partial^2 \psi^w}{\partial x^2} \right)^T \frac{\partial^2 [\psi^w]}{\partial x^2} dx + \int_0^{L_e} GAl^2 \left(\frac{\partial^2 \psi^w}{\partial x^2} \right)^T \frac{\partial^2 [\psi^w]}{\partial x^2} dx$$

$$= \frac{EI}{L_e^3} \begin{bmatrix} 12 & 6L_e & -12 & 6L_e \\ 6L_e & 4L_e^2 & -6L_e & 2L_e^2 \\ -12 & -6L_e & 12 & -6L_e \\ 6L_e & 2L_e^2 & -6L_e & 4L_e^2 \end{bmatrix} + \frac{GAl^2}{L_e^3} \begin{bmatrix} 12 & 6L_e & -12 & 6L_e \\ 6L_e & 4L_e^2 & -6L_e & 2L_e^2 \\ -12 & -6L_e & 12 & -6L_e \\ 6L_e & 2L_e^2 & -6L_e & 4L_e^2 \end{bmatrix}$$

(9)

By assembling the K_u and K_w matrices given above, the stiffness matrix of a nanoframe

element is obtained as follows:

$$\bar{K} = \begin{bmatrix} \frac{EA}{L_e} & 0 & 0 & -\frac{EA}{L_e} & 0 & 0 \\ 0 & 12\frac{EI}{L_e^3}+12\frac{GAl^2}{L_e^3} & 6\frac{EI}{L_e^2}+6\frac{GAl^2}{L_e^2} & 0 & -12\frac{EI}{L_e^3}-12\frac{GAl^2}{L_e^3} & 6\frac{EI}{L_e^2}+6\frac{GAl^2}{L_e^2} \\ 0 & 6\frac{EI}{L_e^2}+6\frac{GAl^2}{L_e^2} & 4\frac{EI}{L_e}+4\frac{GAl^2}{L_e} & 0 & -6\frac{EI}{L_e^2}-6\frac{GAl^2}{L_e^2} & 2\frac{EI}{L_e}+2\frac{GAl^2}{L_e} \\ -\frac{EA}{L_e} & 0 & 0 & \frac{EA}{L_e} & 0 & 0 \\ 0 & -12\frac{EI}{L_e^3}-12\frac{GAl^2}{L_e^3} & -6\frac{EI}{L_e^2}-6\frac{GAl^2}{L_e^2} & 0 & 12\frac{EI}{L_e^3}+12\frac{GAl^2}{L_e^3} & -6\frac{EI}{L_e^2}-6\frac{GAl^2}{L_e^2} \\ 0 & 6\frac{EI}{L_e^2}+6\frac{GAl^2}{L_e^2} & 2\frac{EI}{L_e}+2\frac{GAl^2}{L_e} & 0 & -6\frac{EI}{L_e^2}-6\frac{GAl^2}{L_e^2} & 4\frac{EI}{L_e}+4\frac{GAl^2}{L_e} \end{bmatrix} \tag{10}$$

The above matrix includes both bending and axial effects. Buckling, vibration and bending analysis of nanobeams via matrices that include these both effects were presented by Akbaş [20] using modified couple stress theory. This matrix, which can be used for the solution of a straight nanobeam, is used for the elements of the nanoframe in this study. As it is known, frame systems are structures formed by connecting more than one element to each other at different angles. In order to realize the solutions of these structures, we should first write them on the same axis set, taking into account the orientations of all the elements. For this, transformation matrix (*T*) is used [22, 57]:

$$T = \begin{bmatrix} C & S & 0 & 0 & 0 & 0 \\ -S & C & 0 & 0 & 0 & 0 \\ 0 & 0 & 1 & 0 & 0 & 0 \\ 0 & 0 & 0 & C & S & 0 \\ 0 & 0 & 0 & -S & C & 0 \\ 0 & 0 & 0 & 0 & 0 & 1 \end{bmatrix} \tag{11}$$

C and S define cosine and sine, respectively. C and S are the angle between the local axis of the element and the global axis. To obtain the global stiffness matrix for a nanoframe element, we need to utilize the following equation [22, 55, 57]:

$$K_{mcst} = T^T \bar{K} T \tag{12}$$

The stiffness matrix of a single element of the frame system obtained the following form when the transformation matrix and equation (12) are used:

$$K_{mcst} = \begin{bmatrix} K_{11} & K_{12} & K_{13} & K_{14} & K_{15} & K_{16} \\ K_{21} & K_{22} & K_{23} & K_{24} & K_{25} & K_{26} \\ K_{31} & K_{32} & K_{33} & K_{34} & K_{35} & K_{36} \\ K_{41} & K_{42} & K_{43} & K_{44} & K_{45} & K_{46} \\ K_{51} & K_{52} & K_{53} & K_{54} & K_{55} & K_{56} \\ K_{61} & K_{62} & K_{63} & K_{64} & K_{65} & K_{66} \end{bmatrix} \tag{13}$$

The elements of K_{mcst} matrix are given as follows:

$$K_{11} = K_{44} = \frac{EA}{L_e}C^2 + \left(12\frac{EI}{L_e^3} + 12\frac{GAl^2}{L_e^3}\right)S^2 \tag{14}$$

$$K_{12} = K_{21} = \frac{EA}{L_e}CS - \left(12\frac{EI}{L_e^3} + 12\frac{GAl^2}{L_e^3}\right)CS \tag{15}$$

$$K_{13} = K_{31} = -\left(6\frac{EI}{L_e^2} + 6\frac{GAl^2}{L_e^2}\right)S \tag{16}$$

$$K_{14} = K_{41} = -\frac{EA}{L_e}C^2 - \left(12\frac{EI}{L_e^3} + 12\frac{GAl^2}{L_e^3}\right)S^2 \tag{17}$$

$$K_{15} = K_{51} = -\frac{EA}{L_e}CS + \left(12\frac{EI}{L_e^3} + 12\frac{GAl^2}{L_e^3}\right)CS \tag{18}$$

$$K_{16} = K_{61} = -\left(6\frac{EI}{L_e^2} + 6\frac{GAl^2}{L_e^2}\right)S \tag{19}$$

$$K_{22} = K_{55} = \left(12\frac{EI}{L_e^3} + 12\frac{GAl^2}{L_e^3}\right)C^2 + \frac{EA}{L_e}S^2 \tag{20}$$

$$K_{23} = K_{32} = K_{26} = K_{62} = \left(6\frac{EI}{L_e^2} + 6\frac{GAl^2}{L_e^2}\right)C \tag{21}$$

$$K_{24} = K_{42} = \left(12\frac{EI}{L_e^3} + 12\frac{GAl^2}{L_e^3}\right)CS - \frac{EA}{L_e}CS \tag{22}$$

$$K_{25} = K_{52} = -\left(12\frac{EI}{L_e^3} + 12\frac{GAl^2}{L_e^3}\right)C^2 - \frac{EA}{L_e}S^2 \tag{23}$$

$$K_{33} = K_{66} = 4\frac{EI}{L_e} + 4\frac{GAl^2}{L_e} \tag{24}$$

$$K_{34} = K_{43} = K_{46} = K_{64} = \left(6\frac{EI}{L_e^2} + 6\frac{GAl^2}{L_e^2}\right)S \tag{25}$$

$$K_{35} = K_{53} = K_{56} = K_{65} = -\left(6\frac{EI}{L_e^2} + 6\frac{GAl^2}{L_e^2}\right)C \tag{26}$$

$$K_{36} = K_{63} = \left(2\frac{EI}{L_e} + 2\frac{GAl^2}{L_e}\right) \tag{27}$$

$$K_{45} = K_{54} = -\left(12\frac{EI}{L_e^3} + 12\frac{GAl^2}{L_e^3}\right)CS + \frac{EA}{L_e}CS \tag{28}$$

As can be understood, the matrix given in equation (13) is the stiffness matrix of a nanoframe element based on the modified couple stress theory. In this size-dependent stiffness matrix, besides the material length scale parameter l, there are C and S expressions. If we neglect the material length scale parameter in the stiffness matrix based on the modified couple stress theory, the stiffness matrix based on the classical elasticity theory is obtained. The stiffness matrix of a classical frame element is as follows [57]

$$K_{cl} = \frac{E}{L_e}\begin{bmatrix} AC^2 + \frac{12I}{L_e^2}S^2 & \left(A - \frac{12I}{L_e^2}\right)CS & -\frac{6I}{L_e}S & -\left(AC^2 + \frac{12I}{L_e^2}S^2\right) & -\left(A - \frac{12I}{L_e^2}\right)CS & -\frac{6I}{L_e}S \\ \left(A - \frac{12I}{L_e^2}\right)CS & AS^2 + \frac{12I}{L_e^2}C^2 & \frac{6I}{L_e}C & -\left(A - \frac{12I}{L_e^2}\right)CS & -\left(AS^2 + \frac{12I}{L_e^2}C^2\right) & \frac{6I}{L_e}C \\ -\frac{6I}{L_e}S & \frac{6I}{L_e}C & 4I & \frac{6I}{L_e}S & -\frac{6I}{L_e}C & 2I \\ -\left(AC^2 + \frac{12I}{L_e^2}S^2\right) & -\left(A - \frac{12I}{L_e^2}\right)CS & \frac{6I}{L_e}S & AC^2 + \frac{12I}{L_e^2}S^2 & \left(A - \frac{12I}{L_e^2}\right)CS & \frac{6I}{L_e}S \\ -\left(A - \frac{12I}{L_e^2}\right)CS & -\left(AS^2 + \frac{12I}{L_e^2}C^2\right) & -\frac{6I}{L_e}C & \left(A - \frac{12I}{L_e^2}\right)CS & AS^2 + \frac{12I}{L_e^2}C^2 & -\frac{6I}{L_e}C \\ -\frac{6I}{L_e}S & \frac{6I}{L_e}C & 2I & \frac{6I}{L_e}S & -\frac{6I}{L_e}C & 4I \end{bmatrix} \tag{29}$$

4. Application Procedure

A finite element solution of nodal displacement and rotation analysis based on modified couple stress theory of a nanoscale frame structure is shown. As can be understood from the previous formulations, the size effect takes place in the stiffness matrix. In the solution based on the modified couple stress theory, only the stiffness matrix is affected by the material length scale parameter, which gives the size effect. To perform the solution of a nanoframe system like in Figure 1, first the stiffness matrix of each element is obtained. Then these stiffness matrices are assembled. A global nodal force vector and a global nodal displacement vector are written.

$$\left[K_{mcst}^{global}\right]_{12x12}\begin{Bmatrix} d_{1x} \\ d_{1y} \\ \theta_1 \\ d_{2x} \\ d_{2y} \\ \theta_2 \\ d_{3x} \\ d_{3y} \\ \theta_3 \\ d_{4x} \\ d_{4y} \\ \theta_4 \end{Bmatrix} = \begin{Bmatrix} f_{1x} \\ f_{1y} \\ M_1 \\ f_{2x} \\ f_{2y} \\ M_2 \\ f_{3x} \\ f_{3y} \\ M_3 \\ f_{4x} \\ f_{4y} \\ M_4 \end{Bmatrix} \tag{30}$$

In the above equation, d and θ indicate the nodal displacements and rotations, respectively. In the global nodal force vector, those expressed by f and M are the applied nodal force and moment, respectively. The numbers (*1,2,3,4*) given as subscript indicate the node number. As a final process, the boundary conditions are applied to the required nodes and the results are obtained.

5. Numerical Result and Discussion

In this section of the study, a numerical application is realized. For this purpose, it is assumed that the elements of the nanoframe given in figure 1 are composed of silicon carbide nanotubes. The Young's modulus and Poisson's ratio of silicon carbide nanotube are as follows: *E=0.45 TPa*, *v=0.27* [58, 59]. The shear modulus of silicon carbide nanotube is calculated by the following relation:

$$G = \frac{E}{2(1+v)} \tag{31}$$

The geometric properties of the beam and columns that build up the nanoframe are equal to each other. The length of the nanoframe elements is *L=10 nm*, while their diameter is *d=1 nm*. Lastly, the nodal force and nodal moment are: $f_{2x}=1$ *nN*, $M_3=10$ *nNnm*.

Numerical results are given in normalized form to show the effect of material length scale parameter. Normalized displacements and rotations are expressed as the ratio of the results obtained with the modified couple stress theory to the results obtained with the classical theory of elasticity (*CL*). The material length scale parameter values are changed from 0 nm to 0.5 nm in 0.1 increments. It should be reminded once again that if material length scale parameter set to zero, the solution gives the results of classical elasticity theory. Figure 2 shows the x-direction normalized displacements of node 2 and node 3, while figure 3 shows those in the y-direction. As can be seen figure 2, as the material length scale parameter value increases, there is a decrease in the normalized displacement values. This means that higher

displacements occur when the size effect is not taken into account. In other words, lower displacements occur for the x-direction when the size effect is considered. In Figure 3, the effect of the material length scale parameter on displacement in the y-direction is shown. When the normalized displacement values are examined, it is understood that the effect of the material length scale parameter on the displacements in the y-direction is much less. Figure 4 is plotted to examine the effect of the small scale parameter on nodal rotations. It is understood from this figure that the modified couple stress theory reduces the rotation values. As the material length scale parameter increases, the rotation values decrease.
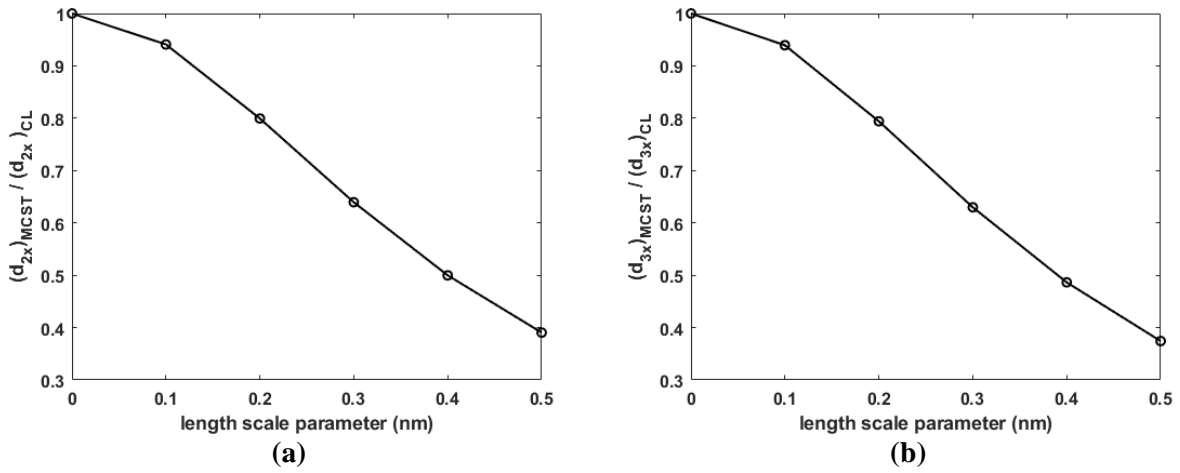

(a)   (b)

Fig.2. The x-direction normalized displacements a) node 2 b) node 3

(a)   (b)
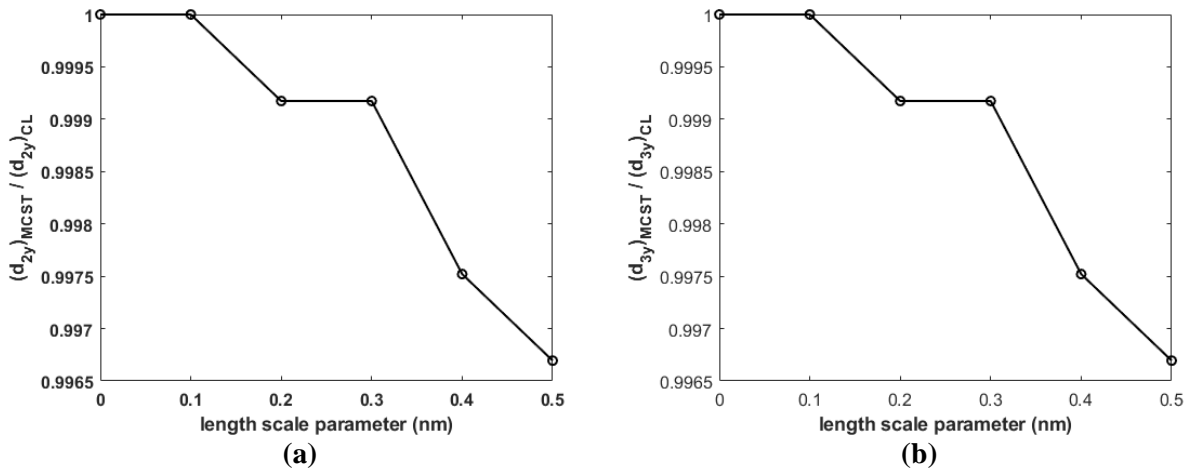
Fig.3. The y-direction normalized displacements a) node 2 b) node 3
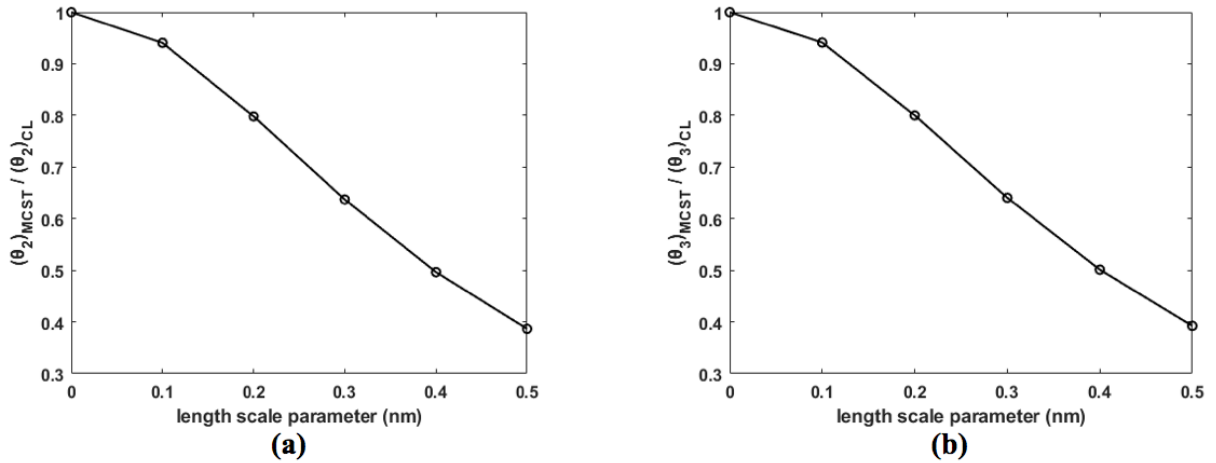
Fig.4. The normalized rotations a) node 2 b) node 3

6. Conclusions

In this work, a size-dependent finite element formulation of nanoframe is presented in the context of the modified couple stress theory. It is important to carry out theoretical analyzes that can reflect correct and actual behaviors of nanoscale structures. Theoretical analyzes have several advantages in terms of both time and cost. When literature is reviewed, it can be seen that the majority of the analyses are on one-dimensional nanoscale elements. This work presents a finite element solution that gives nodal displacements and rotations of a two-dimensional nanoscale frame. Modified couple stress theory, which is one of the elasticity theories that can theoretically present small-scale effects, is the subject of this study. The importance of the material length scale parameter is demonstrated in many scientific articles. When the results of this study are examined, it is understood that the size effect based on the material length scale parameter is important for bending of nanoframe system. Knowing how the material length scale parameter is included in the calculations for the solution of a frame system is important for engineering and device applications of such structures via obtaining numerical result.

References

[1] Iijima, S., Helical microtubules of graphitic carbon, *Nature*, 354(6348), 56-58, 1991.

[2] Becknell, N., Son, Y., Kim, D., Li, D., Yu, Y., Niu, Z., ... and Yang, P., Control of architecture in rhombic dodecahedral Pt–Ni nanoframe electrocatalysts. *Journal of the American Chemical Society*, 139(34), 11678-11681, 2017.

[3] Mahmoud, M.A., Qian, W., and El-Sayed, M.A., Following charge separation on the nanoscale in Cu2O–Au nanoframe hollow nanoparticles. *Nano letters*, 11(8), 3285-3289, 2011.

[4] Zhu, X., Huang, L., Wei, M., Tsiakaras, P., and Shen, P.K., Highly stable Pt-Co nanodendrite in nanoframe with Pt skin structured catalyst for oxygen reduction electrocatalysis. *Applied Catalysis B: Environmental*, 281, 119460, 2021.

[5] Arefi, M., Firouzeh, S., Bidgoli, E.M.R., and Civalek, Ö., Analysis of porous micro-plates reinforced with FG-GNPs based on Reddy plate theory. *Composite Structures*, 247, 112391, 2020.

[6] Esen, I., Abdelrahman, A.A., and Eltaher, M.A. On vibration of sigmoid/symmetric functionally graded nonlocal strain gradient nanobeams under moving load. *International Journal of Mechanics and Materials in Design*, 1-22, 2021.

[7] Esen, I., Abdelrhmaan, A.A., and Eltaher, M.A. Free vibration and buckling stability of FG nanobeams exposed to magnetic and thermal fields. *Engineering with Computers*, 1-20, 2021.

[8] Jena, S.K., Chakraverty, S., and Malikan, M. Vibration and buckling characteristics of nonlocal beam placed in a magnetic field embedded in Winkler–Pasternak elastic foundation using a new refined beam theory: an analytical approach. *The European Physical Journal Pl*us, 135(2), 1-18, 2020.

[9] Akgöz, B., and Civalek, Ö., Thermo-mechanical buckling behavior of functionally graded microbeams embedded in elastic medium. *International Journal of Engineering Science*, 85, 90-104, 2014.

[10] Akgöz, B., and Civalek, Ö., A microstructure-dependent sinusoidal plate model based on the strain gradient elasticity theory. *Acta mechanica*, 226(7), 2277-2294, 2015.

[11] Rahmani, O., Hosseini, S.A.H., Ghoytasi, I., and Golmohammadi, H., Free vibration of deep curved FG nano-beam based on modified couple stress theory. *Steel and Composite Structures*, 26(5), 607-20, 2018.

[12] Yayli, M.Ö., Torsional vibration analysis of nanorods with elastic torsional restraints using non-local elasticity theory. *Micro & Nano Letters*, 13(5), 595-599, 2018.

[13] Yaylı, M.Ö., Uzun, B., and Deliktaş, B., Buckling analysis of restrained nanobeams using strain gradient elasticity. *Waves in Random and Complex Media*, 1-20, 2021.

[14] Uzun, B., Kafkas, U., and Yaylı, M.Ö., Axial dynamic analysis of a Bishop nanorod with arbitrary boundary conditions. *ZAMM-Journal of Applied Mathematics and Mechanics/Zeitschrift für Angewandte Mathematik und Mechanik*, 100(12), e202000039, 2020.

[15] Uzun, B., Kafkas, U., and Yaylı, M.Ö., Stability analysis of restrained nanotubes placed in electromagnetic field. *Microsystem Technologies*, 26(12), 3725-3736, 2020.

[16] Yaylı, M.Ö., Stability analysis of gradient elastic microbeams with arbitrary boundary conditions. *Journal of Mechanical Science and Technology*, 29(8), 3373-3380, 2015.

[17] Yayli, M.Ö., On the axial vibration of carbon nanotubes with different boundary conditions. *Micro & Nano Letters*, 9(11), 807-811, 2014.

[18] Uzun, B., Kafkas, U., and Yaylı, M.Ö., Free vibration analysis of nanotube based sensors including rotary inertia based on the Rayleigh beam and modified couple stress theories. *Microsystem Technologies,* 27(5), 1913-1923, 2021.

[19] Yayli, M.O., Stability analysis of a gradient elastic beam using finite element method. *International Journal of Physical Science*, 6(12), 2844-2851, 2011.

[20] Akbaş, Ş.D., Static, Vibration, and Buckling Analysis of Nanobeams (pp. 123-137). InTech, 2017.

[21] Numanoğlu, H.M., Thermal Vibration of Zinc Oxide Nanowires by using Nonlocal Finite Element Method. *International Journal of Engineering and Applied Sciences*, 12(3), 99-110, 2020.

[22] Numanoğlu, H.M., Examination of How Size-Effect Modifies the Stiffness and Mass Matrices of Nanotrusses/Nanoframes. *International Journal of Engineering and Applied Sciences*, 13(4), 155-165, 2021.

[23] Uzun, B., and Yaylı, M.Ö., Nonlocal vibration analysis of Ti-6Al-4V/ZrO2 functionally graded nanobeam on elastic matrix. *Arabian Journal of Geosciences*, 13(4), 1-10, 2020.

[24] Uzun, B., Yaylı, M.Ö., and Deliktaş, B., Free vibration of FG nanobeam using a finite-element method. *Micro & Nano Letters*, 15(1), 35-40, 2020.

[25] Uzun, B., and Yayli, M.Ö., A solution method for longitudinal vibrations of functionally graded nanorods. *International Journal of Engineering and Applied Sciences*, 12(2), 78-87, 2020.

[26] Akbaş, Ş.D., Forced vibration analysis of cracked nanobeams. *Journal of the Brazilian Society of Mechanical Sciences and Engineering*, 40(8), 1-11, 2018.

[27] Akbas, S.D., Forced vibration analysis of cracked functionally graded microbeams. *Advances in Nano Research*, 6(1), 39, 2018.

[28] Karamanli, A. Structural behaviours of zigzag and armchair nanobeams using finite element doublet mechanics. *European Journal of Mechanics-A/Solids*, 89, 104287, 2021.

[29] Eltaher, M.A., Khairy, A., Sadoun, A.M., and Omar, F.A. Static and buckling analysis of functionally graded Timoshenko nanobeams. *Applied Mathematics and Computation*, 229, 283-295, 2014.

[30] Akbaş, Ş.D., Axially forced vibration analysis of cracked a nanorod. *Journal of Computational Applied Mechanics*, 50(1), 63-68, 2019.

[31] Numanoğlu, H. M., Akgöz, B., and Civalek, Ö., On dynamic analysis of nanorods. *International Journal of Engineering Science*, 130, 33-50, 2018.

[32] Ebrahimi, F., Shafiei, N., Kazemi, M., and Mousavi Abdollahi, S.M., Thermo-mechanical vibration analysis of rotating nonlocal nanoplates applying generalized differential quadrature method. *Mechanics of Advanced Materials and Structures*, 24(15), 1257-1273, 2017.

[33] Khaniki, H.B., and Hosseini-Hashemi, S., Dynamic transverse vibration characteristics of nonuniform nonlocal strain gradient beams using the generalized differential quadrature method. *The European Physical Journal Plus*, 132(11), 1-15, 2017.

[34] Najafzadeh, M., Adeli, M.M., Zarezadeh, E., and Hadi, A., Torsional vibration of the porous nanotube with an arbitrary cross-section based on couple stress theory under magnetic field. *Mechanics Based Design of Structures and Machines*, 1-15, 2020.

[35] Shafiei, N., and Kazemi, M., Nonlinear buckling of functionally graded nano-/micro-scaled porous beams. *Composite Structures*, 178, 483-492, 2017.

[36] Shojaeefard, M.H., Googarchin, H.S., Ghadiri, M., and Mahinzare, M., Micro temperature-dependent FG porous plate: Free vibration and thermal buckling analysis using modified couple stress theory with CPT and FSDT. *Applied Mathematical Modelling*, 50, 633-655, 2017.

[37] Xue, Y., Jin, G., Ma, X., Chen, H., Ye, T., Chen, M., and Zhang, Y., Free vibration analysis of porous plates with porosity distributions in the thickness and in-plane directions using isogeometric approach. *International Journal of Mechanical Sciences*, 152, 346-362, 2019.

[38] Akbaş, Ş.D., Stability of a non-homogenous porous plate by using generalized differantial quadrature method. *International Journal of Engineering and Applied Sciences*, 9(2), 147-155, 2017.

[39] Chen, D., Yang, J., and Kitipornchai, S., Buckling and bending analyses of a novel functionally graded porous plate using Chebyshev-Ritz method. *Archives of Civil and Mechanical Engineering*, 19(1), 157-170, 2019.

[40] Jena, S. K., Chakraverty, S., and Malikan, M., Application of shifted Chebyshev polynomial-based Rayleigh–Ritz method and Navier's technique for vibration analysis of a functionally graded porous beam embedded in Kerr foundation. *Engineering with Computers*, 1-21, 2020.

[41] Tang, H., Li, L., and Hu, Y., Buckling analysis of two-directionally porous beam. *Aerospace Science and Technology*, 78, 471-479, 2018.

[42] Civalek, Ö., and Kiracioglu, O., Free vibration analysis of Timoshenko beams by DSC method. *International Journal for Numerical Methods in Biomedical Engineering*, 26(12), 1890-1898, 2010.

[43] Civalek, Ö., and Avcar, M., Free vibration and buckling analyses of CNT reinforced laminated non-rectangular plates by discrete singular convolution method. *Engineering with Computers*, 1-33, 2020.

[44] Bouazza, M., and Zenkour, A.M., Vibration of carbon nanotube-reinforced plates via refined n th-higher-order theory. *Archive of Applied Mechanics*, 90(8), 1755-1769, 2020.

[45] Chaabane, L. A., Bourada, F., Sekkal, M., Zerouati, S., Zaoui, F. Z., Tounsi, A., ... and Tounsi, A., Analytical study of bending and free vibration responses of functionally graded beams resting on elastic foundation. *Structural Engineering and Mechanics*, 71(2), 185-196, 2019.

[46] Li, L., Li, X., and Hu, Y., Nonlinear bending of a two-dimensionally functionally graded beam. *Composite Structures*, 184, 1049-1061, 2018.

[47] Ghayesh, M.H., Nonlinear vibration analysis of axially functionally graded shear-deformable tapered beams. *Applied Mathematical Modelling*, 59, 583-596, 2018.

[48] Kahya, V., and Turan, M., Finite element model for vibration and buckling of functionally graded beams based on the first-order shear deformation theory. *Composites Part B: Engineering*, 109, 108-115, 2017.

[49] Kahya, V., and Turan, M., Vibration and buckling of laminated beams by a multi-layer finite element model. *Steel and Composite Structures*, 28(4), 415-426, 2018.

[50] Akbaş, Ş.D., Free vibration of axially functionally graded beams in thermal environment. *International Journal of Engineering and Applied Sciences*, 6(3), 37-51, 2014.

[51] Civalek, Ö., Geometrically nonlinear dynamic and static analysis of shallow spherical shell resting on two-parameters elastic foundations. *International Journal of Pressure Vessels and Piping*, 113, 1-9, 2014.

[52] Civalek, Ö., and Baltacıoglu, A.K., Free vibration analysis of laminated and FGM composite annular sector plates. *Composites Part B: Engineering*, 157, 182-194, 2019.

[53] Mercan, K., Demir, Ç., and Civalek, Ö., Vibration analysis of FG cylindrical shells with power-law index using discrete singular convolution technique. *Curved and Layered Structures*, 3(1), 2016.

[54] Civalek, Ö., Akbaş, Ş.D., Akgöz, B., and Dastjerdi, S., Forced vibration analysis of composite beams reinforced by carbon nanotubes. *Nanomaterials*, 11(3), 571, 2021.

[55] Koçyiğit, K., and Akbaş, Ş.D., Çatlak içeren bir çerçeve taşıyıcı sistemin zorlanmış titreşim analizi. *Politeknik Dergisi*, 23(4), 1059-1071, 2020.

[56] Yang, F.A.C.M., Chong, A.C.M., Lam, D.C.C., and Tong, P., Couple stress based strain gradient theory for elasticity. *International journal of solids and structures*, 39(10), 2731-2743, 2002.

[57] Logan, D.L., A first course in the finite element method. Cengage Learning, 2016.

[58] Latu-Romain, L., and Ollivier, M., Silicon carbide one-dimensional nanostructures. John Wiley & Sons, 2015.

[59] Petrushenko, I.K., and Petrushenko, K.B., Mechanical properties of carbon, silicon carbide, and boron nitride nanotubes: effect of ionization. *Monatshefte für Chemie-Chemical Monthly*, 146(10), 1603-1608, 2015.

Numerical Elastic Analysis of Functionally Graded (FG) Polar Orthotropic and Exponentially Varying-Thickness Rotating Disks via Combined Complementary Functions and the Transfer Matrix Methods

Vebil Yıldırım

Dept. of Mechanical Engineering, University of Çukurova, 01330 Adana, Turkey
E-mail address: vebil@cu.edu.tr

ORCID number of the author:
0000-0001-9955-8423

Abstract

In the present paper, the transfer matrix method (TMM) is to be employed for the first time in the open literature for the elastic analysis of variable-thickness disks made of functionally graded (FG) two orthotropic materials. Those materials are assumed to be continuously radially functionally graded (FG) based on the Voigt rule of mixture with two models. An exponential disk profile with two parameters is considered. Effects of the different boundary conditions (free-free, fixed-free, and fixed-fixed) and inhomogeneity indexes on the elastic response of the disk rotating at a constant angular speed are also examined. Additionally, direct numerical solutions of the problem with the complementary functions method (CFM) are presented in tabular forms together with the transfer matrix method solutions in which CFM was used as an assistant tool. It was observed that both location and amplitude of the maximum equivalent stress are affected by the grading models chosen. Such differences become more obvious for small values of the inhomogeneity indexes. The maximum relative error may reach 18% for the two material grading models in fixed-free disks. Consequently, Model-I may be recommended for just the inhomogeneity indexes equal to or greater than 0.5.

Keywords: Rotating disk, functionally graded, polar orthotropic, variable thickness, transfer matrix method, complementary functions method, initial value problem.

1. Introduction

Rotating disks are essential elements of turbine rotors, compressors, flywheels, automobile disc brake systems, gears, etc. Today's scientific works focus on the use of advanced materials so that discs can withstand much higher rotational speeds and resulting stresses.

To serve the purpose above mentioned, ordinary anisotropic materials have been examined [1-24]. The mechanical benefits of a material gradient may be significant in the design of such structures to enhance structural performance. As a class of nonhomogeneous isotropic advanced materials, low-cost functionally graded (FG) metal-ceramics play a significant role in this subject area [25-51]. Based on a chosen material grading rule, material properties may vary continuously along with one or more certain directions in FG metal-ceramics. From those, Eraslan and Akış [28] worked on the elastic analysis of FG parabolically-varying thickness disks. Based on a semi-analytical axisymmetric elastic solution, Bayat et al. [31] considered rotating hollow parabolic and hyperbolic disks. Hojjati and Jafari [34] introduced two analytical methods, namely the homotopy perturbation method (HPM) and Adomian's decomposition method (ADM), to obtain stresses and displacements in rotating disks with

variable thicknesses and densities. They also compared the result with the verified variational iteration method (VIM) solution. The comparison among the methods used in Ref. [34] showed that although the numerical results were almost the same, HPM is much easier, more convenient, and more efficient than ADM and VIM. Hojjati and Hassani [35] conducted a stress-strain analysis of rotating discs with nonuniform thickness and density for an elastic–linear hardening disk material. They used variable material properties (VMP) theory for a theoretical solution, Runge–Kutta's method for a numerical solution, and commercial finite element modeling for comparisons of their results. They suggested the VMP method which provides reliable means for complex discs. Nie and Batra [36] analyzed axisymmetric deformations of a rotating FGM nonuniform disk made of a rubberlike material that was modeled as isotropic, linear thermoelastic, and incompressible by using an Airy stress function and the differential quadrature method. They [36] also worked on the material tailoring for obtaining a constant linear combination of the hoop stress and the radial stress. By dividing the variable-thickness disk into sub-domains with uniform thickness, Hassani et al. [38] studied the elastic behavior of rotating FG- isotropic hyperbolic rotating disks based on of a semi-exact method of Liao's homotopy analysis. Nejad et al. [41-42] examined exponentially FG disks subjected to internal and external pressures [41] and centrifugal forces [42]. Yıldırım [44] analytically formulated the exact elastic response of a power-law graded hyperbolic rotating disk subjected to the internal and external pressures including a rotation at a constant angular velocity under four physical boundary conditions. Based on both complementary functions and transfer matrix methods, Yıldırım and Kacar [45] introduced a versatile computer package program for the elastic analysis of arbitrarily FG-isotropic thick-walled annular structures under all possible boundary conditions, namely variable thickness disks, cylinders, and spheres. Gang [47] analytically studied the stress analysis of a simple-power law graded hyperbolic free-free rotating disk for four convergent disk profiles and negative inhomogeneity indexes. Yıldırım [48] presented a comprehensive parametric study for a power-law graded hyperbolic rotating disk. Based on the transfer matrix approach, Yıldırım [49], considered six different material grading rules such as a simple power rule (P-FGM), an exponential function (E-FGM), a linear function (L-FGM), a Voigt mixture rule with the power of volume fractions of constituents (V-FGM), a Mori-Tanaka scheme (MT-FGM), and a sigmoid function (S-FGM) with several parabolically/linearly/hyperbolically tapered disk profiles including uniform ones to study the elastic response of rotating disks made of FG metal and ceramic pairs (*Al/Al$_2$O$_3$*) under free-free, fixed-free, and fixed-fixed boundary conditions. The computer program introduced in [45] was used in Yıldırım's [49] study, and the transfer matrix was obtained with the help of the complementary functions method as in the present study. Khorsand and Tang [50], recently, employed an advanced algorithm to optimize the weight of a hollow FG varied thickness disk under thermoelastic loads based on a combination of a co-evolutionary particle swarm optimization (CPSO) approach coupled with a differential quadrature (DQ).

In quest of searching for more advanced materials, the mechanical benefits of a material gradient have begun to be probed into anisotropic materials [51-61] instead of isotropic ones [25-50]. This group of materials, which are mainly in the scope of the present study, are called functionally graded (FG) anisotropic materials or are referred to as anisotropic and inhomogeneous materials. There are, unfortunately, a very limited number of works on FG disks composed of anisotropic materials in the open literature [51-61]. Among these, Durodola and Attia [51] studied elastic stresses in a rotating hollow uniform disk made from FG orthotropic materials. Chen et al. [52] presented a 3-D analytical solution for a uniform transversely isotropy exponentially FG rotating disk. Nie et al. [53] calculated numerically the required radial variation of the volume fraction of fibers for a rotating annular CR-disk composed of a fiber-reinforced composite. Kansal and Parvez [54] carried out stress analysis of orthotropic graded rotating annular disks under a parabolic temperature distribution. Lubarda [55] worked on the elastic response of uniformly pressurized cylindrically anisotropic hollow

16

uniform thin rotating disks by using both the finite difference method and a Fredholm integral equation. Peng and Li [56] also employed a Fredholm integral equation for elastic analysis of a hollow FG polar-orthotropic rotating disk under free-free and fixed-free boundary conditions. After deriving a confluent hypergeometric differential equation, Essa and Argeso [58] studied analytically and numerically the effects of the anisotropy degree on the elastic fields of polar orthotropic FG annular free-free and fixed-free rotating variable-thickness disks. Based on the finite difference method and Voigt mixture grading rule with powers, Zheng et al. [59] numerically studied elastic fields in a fiber-matrix FG variable thickness circumferentially aligned (CR) disk mounted on a rotating shaft and subjected to an angular deceleration. Zheng et al.'s [59] study revealed that disk deceleration has no effect on the radial and hoop stresses except the shear stress. As an extension of Ref. [57], Yıldırım [60] proposed closed-form solutions for the elastic fields in a simple power-law graded polar orthotropic hyperbolically tapered disk under separate inner/outer pressures, and centrifugal forces due to the rotation at a constant angular speed. Yıldırım's [60] formulas are capable of exact determination of the elastic behavior of continuously hyperbolically tapered disks made of a single isotropic material, made of a single polar orthotropic material, or made of a nonhomogeneous material formed by functionally power-law graded two isotropic materials, or a nonhomogeneous material formed by functionally power-law graded two orthotropic materials. As the latest study in the related realm, Yıldırım [61] numerically investigated the elastic response of arbitrarily functionally graded polar orthotropic rotating disks having constant thickness. Anisotropy effects on the elastic response were examined numerically with both simple power and exponential material grading rules with the help of only complementary functions method (CFM). CFM solutions were verified with closed-form solutions to simple power gradation rule and uniform disks.

As seen from the open literature that there are just three studies conducted by Essa and Argeso [58], Zheng et al. [59], and Yıldırım [60] on the elastic response of variable-thickness FG polar orthotropic rotating disks. The last work [60] is an analytical study which considers just hyperbolic thickness variation, and the simple-power material grading pattern. This was a great motivation for the author.

This study is a continuation of References [45, 49, 60-61] to study the elastic response of exponentially varying thickness FG polar orthotropic rotating disks based on the combined complementary functions and the transfer matrix methods. As stated above, Yıldırım [49] used the transfer matrix method previously as in the present study for the variable thickness disks (parabolic, hyperbolic, and linearly varying) made of FG two isotropic materials that are metallic and ceramic ($E_r(r) = E_\theta(r) = E(r)$ and $v_{r\theta} = v_{\theta r} = v$). Yıldırım [49] revealed that the free-free and fixed-free variable thickness disks show better performance than the uniform ones under centrifugal forces. The present study also aims to compare the results of the frequently used two Voigt models for the gradation of two orthotropic materials. The author hopes that the findings of the present study will be very helpful to engineers and academicians.

2. Mathematical Formulation and Solution of the Problem

Under small deformations and a state of axisymmetric plane stress assumptions for thin plates, field equations of a variable thickness rotating nonhomogeneous disk made of a linear elastic polar orthotropic material in polar coordinates (r, θ) are reduced to [60]

$$\varepsilon_r(r) = \frac{du_r(r)}{r}, \quad \varepsilon_\theta(r) = \frac{u_r(r)}{r} \tag{1a}$$

$$\sigma_r(r) = -\frac{E_\theta(r)v_{r\theta}}{v_{\theta r}(v_{r\theta}v_{\theta r} - 1)}\varepsilon_r(r) - \frac{E_\theta(r)v_{r\theta}}{(v_{r\theta}v_{\theta r} - 1)}\varepsilon_\theta(r) \tag{1b}$$
$$= C_{11}(r)\varepsilon_r(r) + C_{12}(r)\varepsilon_\theta(r)$$

$$\sigma_\theta(r) = -\frac{E_\theta(r)v_{r\theta}}{(v_{r\theta}v_{\theta r} - 1)}\varepsilon_r(r) - \frac{E_\theta(r)}{(v_{r\theta}v_{\theta r} - 1)}\varepsilon_\theta = C_{12}(r)\varepsilon_r(r) + C_{22}(r)\varepsilon_\theta(r) \tag{1c}$$

$$\big(h(r)r\sigma_r(r)\big)' - h(r)\sigma_\theta(r) + \rho(r)h(r)\omega^2 r = 0 \tag{1d}$$

where Eq. (1a) is called the strain-displacement relations, Eqs. (1b) and (1c) are referred to as linear elastic stress-strain relations, and finally, Eq. (1d) is the equilibrium equation under the centrifugal forces. In Eq. (1), $u_r(r)$ is the radial displacement, $\varepsilon_r(r)$ and $\varepsilon_\theta(r)$ are the radial and circumferential strains, respectively; $\sigma_r(r)$ is the radial stress, $\sigma_\theta(r)$ is the hoop stress, ω is the constant angular velocity, $\rho(r)$ is the material density, $h(r)$ is the disk thickness profile, $E_r(r)$ and $E_\theta(r)$ are Young's moduli along the radial and tangential directions, respectively; $C_{ij}(r)$ are the transformed on-axis in-plane stiffness terms $(E_1 = E_r, E_2 = E_\theta, v_{12} = v_{r\theta})$, in addition $v_{r\theta}$ and $v_{\theta r}$ are anisotropic Poisson's ratios assumed to be constant in the formulation. Those anisotropic Poisson's ratios are also related by Maxwell's theorem as follows

$$\frac{v_{\theta r}}{E_\theta(r)} = \frac{v_{r\theta}}{E_r(r)} \tag{2}$$

It is worth noting that, the radial and circumferential strains must obey the following compatibility equation

$$\frac{d}{dr}\big(r\varepsilon_\theta(r)\big) - \varepsilon_r(r) = 0 \tag{3}$$

Navier equation which is in the form of a second-order differential equation with variable coefficients is derived from the field equations given in Eq. (1) as follows

$$\frac{d^2 u_r(r)}{dr} + \left(\frac{1}{r} + \frac{\frac{dC_{11}(r)}{dr}}{C_{11}(r)} + \frac{\frac{dh(r)}{dr}}{h(r)}\right)\frac{du_r(r)}{dr} + \left(-\frac{C_{22}(r)}{r^2 C_{11}(r)} + \frac{C_{12}(r)}{rC_{11}(r)}\left(\frac{\frac{dC_{11}(r)}{dr}}{C_{11}(r)} + \frac{\frac{dh(r)}{dr}}{h(r)}\right)\right)u_r(r) = -\frac{\rho(r)\omega^2 r}{C_{11}(r)} \tag{4}$$

Equation (4) may be solved by using a technique developed for the solution of two-point boundary value problems (BVP), or it may be handled by a technique like transfer matrix [1,49,62-69] and complementary functions methods [24,61,70-75] or any of the others developed for the solution of initial value problems (IVP).

The principal aim of the present study is to make use of the transfer matrix method in the solution of such kinds of problems. The transfer matrix method allows accurate and economical

solutions to more complicated problems which may be presented in future works. As a by-product, direct solutions to the same problem considered by the complementary functions method are also to be tabulated in the present work.

To employ the transfer matrix method, firstly, Eq. (4) should be written as a first-order differential equation set as follows

$$\frac{du_r(r)}{dr} = -\frac{E_\theta(r)v_{r\theta}}{rE_r(r)}u_r(r) - \frac{(v_{r\theta}v_{\theta r} - 1)}{E_r(r)}\sigma_r(r) \tag{5a}$$

$$\frac{d\sigma_r(r)}{dr} = -\frac{E_\theta(r)(E_r(r) - E_\theta(r)v_{r\theta}^2)}{r^2 E_r(r)(v_{r\theta}v_{\theta r} - 1)}u_r(r) + \left(\frac{E_\theta(r)v_{r\theta}}{rE_r(r)} - \frac{1}{r} - \frac{\frac{dh(r)}{dr}}{h(r)}\right)\sigma_r(r) - \rho(r)\omega^2 r \tag{5b}$$

Equation (5) is written in a more compact form of

$$\frac{dS(r)}{dr} = D(r)S(r) + f(r) \tag{6}$$

where $D(r)$ is the differential matrix, $S(r)$ is the state vector and $f(r)$ is the nonhomogeneous vector.

$$S(r) = \begin{Bmatrix} u_r(r) \\ \sigma_r(r) \end{Bmatrix} \tag{7a}$$

$$f(r) = \begin{Bmatrix} 0 \\ -\rho(r)\omega^2 r \end{Bmatrix} \tag{7b}$$

In the transfer matrix method, the general solution of Eq. (6) is given by [62]

$$S(r) = F(a,r)S(a) + \int_a^r F(\xi,r)f(\xi)d\xi \tag{8}$$

In a few words, If both $F(a,r)$ and $S(a)$ are known in Eq. (8), then both the radial displacement and the radial stress are obtained at any surface of the disk in a straight forward. For the circumferential stress, utilizing Eq. (1), the following may also be written

$$\sigma_\theta(r) = \left(\frac{C_{11}^2(r) - C_{12}^2(r)}{C_{11}(r)}\right)\frac{u_r(r)}{r} + \left(\frac{C_{12}(r)}{C_{11}(r)}\right)\sigma_r(r) \tag{9}$$

On the eve of the application of Eq. (8), both the overall transfer matrix and, then, the unknown elements of the initial state vector, $S(a)$, should be determined. If the elements of the differential matrix are not a function of the radial coordinate, then, it is possible to obtain a closed-form solution for the transfer matrix elements [49, 62, 69]. Otherwise, a numerical solution technique like the complementary functions method as in the present study or any ordinary differential equation set solver in the case of variable coefficients may be used. As

may be guessed from Eq. (5), since the elements of the differential matrix become more complex functions due to the variation of both the material and geometrical properties of the disk, it is suitable to solve directly the related differential equations instead of using some approximate methods to get much more accurate elements of the transfer matrix. Both the material orthotropy [61] and the thickness gradient [49] significantly influence the accuracy of the transfer matrix.

The transfer matrix satisfies a similar differential equation with the state vector in Eq. (6) in case of $f(r) = 0$ 62.

$$\frac{dF(a,r)}{dr} = D(r)F(a,r) \tag{10}$$

The numerical solution of Eq. (10) under Kronecker delta initial boundary conditions gives the transfer matrix in the numerical form [62-63,73-75]

$$F(a,a) = I \tag{11}$$

In Eq. (11), I is the unit matrix. In the present study, the numerical solution of Eq. (10) under boundary conditions given in Eq. (11) was achieved with the help of the complementary functions method whose details were presented in References [24, 61]. This combined technique has already been used successfully in some of the author's previous studies [73-75].
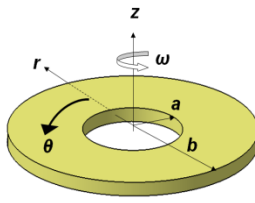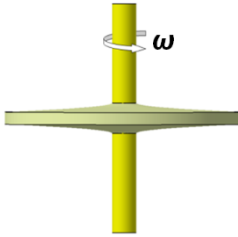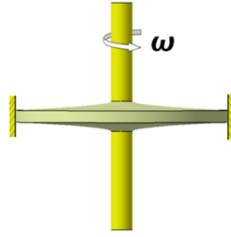
Immediately after the numerical determination of the transfer matrix, the unknown elements of the initial state vector may be established. To do this, Eq. (8) is written at $r = b$, the boundary conditions given at inner and outer surfaces are then implemented into the equation. The boundary conditions considered in the present study are presented in Table 1. After implementation of those boundary conditions, the whole elements of the initial state vector are calculated from the following equations (see Appendix).

$$S(a)_{Free-Free} = \begin{Bmatrix} u_r(a) \\ \sigma_r(a) \end{Bmatrix} = \begin{Bmatrix} \dfrac{\omega^2 \int_a^b F_{2,2}(\xi,r)\rho(\xi)\xi d\xi}{F_{2,1}(a,b)} \\ 0 \end{Bmatrix} \tag{12a}$$

$$S(a)_{Fixed-Free} = \begin{Bmatrix} u_r(a) \\ \sigma_r(a) \end{Bmatrix} = \begin{Bmatrix} 0 \\ \dfrac{\omega^2 \int_a^b F_{2,2}(\xi,r)\rho(\xi)\xi d\xi}{F_{2,2}(a,b)} \end{Bmatrix} \tag{12b}$$

$$S(a)_{Fixed-Fixed} = \begin{Bmatrix} u_r(a) \\ \sigma_r(a) \end{Bmatrix} = \begin{Bmatrix} 0 \\ \dfrac{\omega^2 \int_a^b F_{1,2}(\xi,r)\rho(\xi)\xi d\xi}{F_{1,2}(a,b)} \end{Bmatrix} \tag{12c}$$

Table 1. Boundary conditions considered [44]

Free-Free	Fixed-Free	Fixed-Fixed
$\sigma_r(a) = 0$	$u_r(a) = 0$	$u_r(a) = 0$
$\sigma_r(b) = 0$	$\sigma_r(b) = 0$	$u_r(b) = 0$

3. Verifications of the Results

For the sake of simplicity, the application of this method may be shown on the simple model of Eq. (5) governs the elasto-static behavior of non-uniform disks made of any arbitrarily continuously graded polar orthotropic materials. The disk thickness may vary along the radial coordinate according to any differentiable function.

In the present study, a two-parameter exponential function proposed by Eraslan and Orcan [76] is studied with $a = 0.01m, b = 0.1m$, $h_o = a$, $m = 0.6$, and $k = 0.8$ (Fig. 1).

$$h(r) = h_o e^{-m(\frac{r}{b})^k}$$ (13)

In the present study, a simple Voigt mixture rule is utilized with a power of volume fraction of constituents based on the two models (Fig. 2)

$$V_B^I = \left(\frac{r - a}{b - a}\right)^n, n \geq 0$$ (14a)

$$V_B^{II} = \left(\frac{r^n - a^n}{b^n - a^n}\right), n > 0$$ (14b)
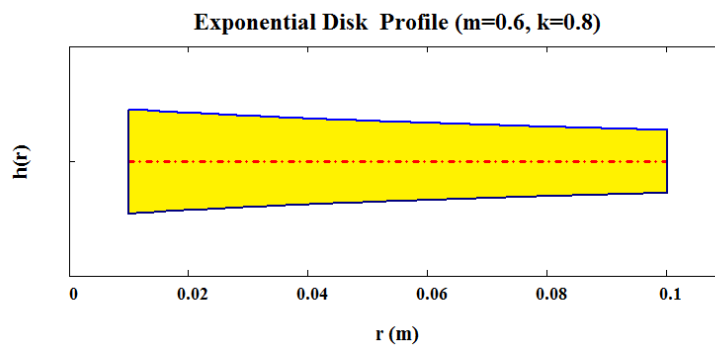
Fig. 1. The exponential disk profile

21

Where n is called the inhomogeneity parameter, V_B stands for the volume fraction of $Material - B$, superscripts show the model number. The radial variation of the effective material properties such as $E_r(r)$, $E_\theta(r)$, and $\rho(r)$ are then defined by the following expression.

$$P(r) = P_A V_A + P_B V_B = P_A(1 - V_B) + P_B V_B = (P_B - P_A)V_B + P_A \tag{15}$$

In Eq. (15), the outer surface is to be $Material - B$ rich (woven Glass fiber/Epoxy prepreg) while the inner surface is $Material - A$ rich (An injection molded Nylon 6 composite containing 40 wt% short glass fiber) (Table 2). The same gradation of Eq. (14b) was originally used by Peng and Li [56] for uniform thickness polar orthotropic FG annular disks.

It is worth noting that, in the present numerical analysis, the arithmetic mean of anisotropic Poisson's ratios of two orthotropic materials is considered.
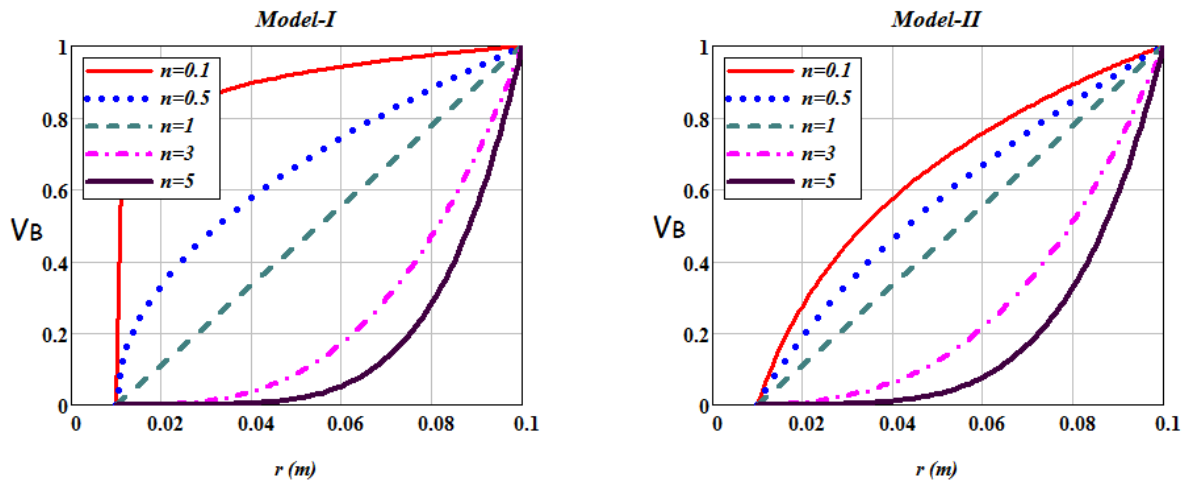
Fig. 2. Volume fraction models considered in this work

Table 2. Anisotropic constituent materials and their properties.

	E_r (GPa)	E_θ(GPa)	ρ (kg/m³)	$\nu_{r\theta}$
$Material - A$ [19-20, 56]	12.0	20.0	1600	0.21
$Material - B$ [19-20]	21.8	26.95	2030	0.15

4. Validation of he Present Formulation

The followings are used for dimensionless displacement and stresses

$$\bar{u}_r = \frac{E_o}{\rho_o \omega^2 b^3}\, u_r, \bar{\sigma}_r = \frac{\sigma_r}{\rho_o \omega^2 b^2}, \bar{\sigma}_\theta = \frac{\sigma_\theta}{\rho_o \omega^2 b^2} \tag{16}$$

In this section, $\sigma_o = 12\ GPa, \rho_o = 1600\ kg/m^3$ have been used in Eq. (16) to calculate the non-dimensional elastic fields in a uniform rotating disk made of FG orthotropic materials having properties given in Table 2. Peng and Li [56] studied this disk of $a/b = 0.4$ by using Model-II in Eq. (14b). The main difference between the present study and Ref. [56] is that the constant value of anisotropic Poisson's ratios is taken differently. That is, Peng and Li [56] used $\nu_{r\theta} = 0.21 = constant$ along the radial coordinate while the present study considers the arithmetic mean of Poisson's ratios, $\nu_{r\theta} = 0.18 = constant$. Since Ref. [56] presented the results in graphical forms, the comparison is to be made in Fig. 3. A perfect harmony can be seen in Fig. 3. Very minor differences in the values of the radial displacement may be due to the value of Poisson's ratio used.
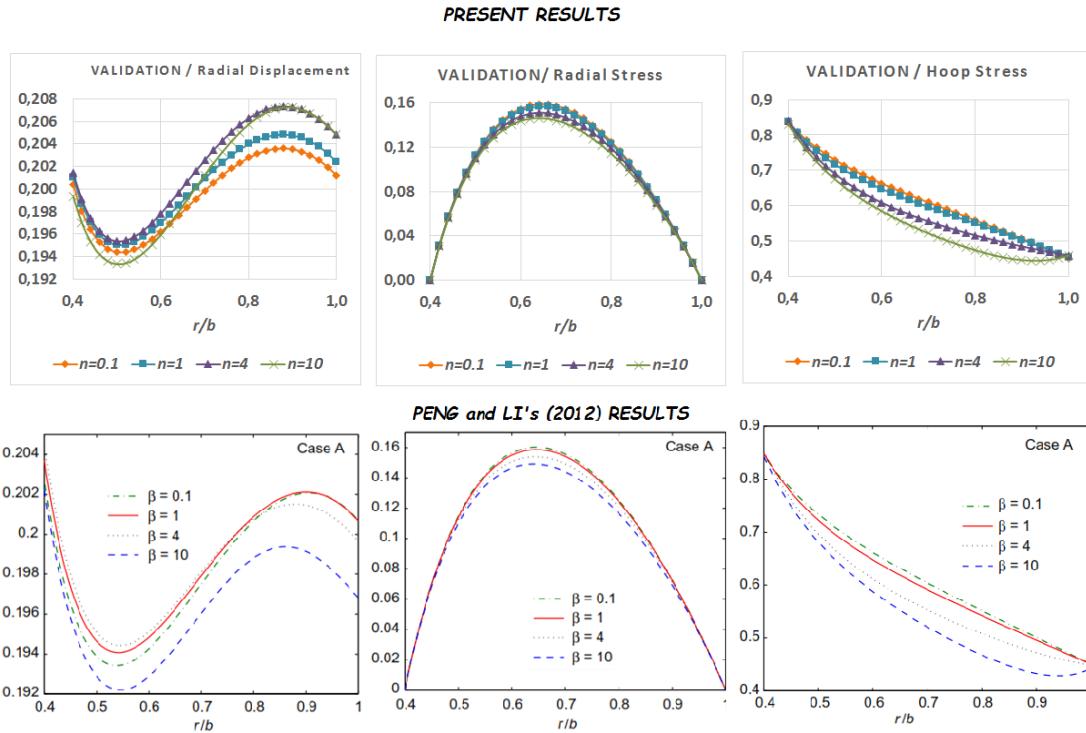
Fig. 3. Validation of the present dimensionless results with the open literature ($\sigma_o = 12GPa. \rho_o = \frac{1600kg}{m^3}$, Free − Free)

5. Numerical Examples

Unless otherwise stated, $\sigma_o = 20GPa, \rho_o = 1600kg/m^3$ are to be used in the calculation of dimensionless quantities in Eq. (16) for a non-uniform disk of $a/b = 0.1$ in this section. Dimensionless elastic fields under free-free, fixed-free, and fixed-fixed boundary conditions are illustrated in Figs. 4-6 based on the two models.

For the aim of comparison of the transfer matrix method (TMM) and the complementary functions method (CFM) solutions for an exponential disk based on the two models with n=3, some numerical results are given in the tabular form in Tables 3 and 4. In those tables, the equivalent von-Mises stress under plane stress assumption is defined by

$$\sigma_{eq} = \sqrt{\sigma_r{}^2 - \sigma_r\sigma_\theta + \sigma_\theta{}^2} \qquad (17)$$

When comparing two models (Fig. 2), minor differences are observed in the variation of the same elastic properties for inhomogeneity indexes greater than the unit. However, when the inhomogeneity index approaches zero, viz., when the inhomogeneity index is strictly less than the unit, the significant differences become obvious. The effects of these on the numerical values of the elastic fields are to be discussed below.

From Figs. 4-6, it is mostly observed that as n increases the maximum displacement also increases while both the maximum radial stress and circumferential stress decrease. Those figures also show that the maximum radial dimensionless displacement is located at the outer surface under both free-free and fixed-free boundary conditions. However, it is in the vicinity of the mid surface, at $r/b \cong 0.6$, for fixed-fixed boundaries. Model-II gives slightly higher maximum radial displacements than Model-I:

$(\bar{u}_r)^I_{max} = 0.195274, \quad (\bar{u}_r)^{II}_{max} = 0.2048695 \quad \rightarrow \quad at \ r = b \ with \ n = 0.1 \ (FREE - FREE)$

$(\bar{u}_r)^I_{max} = 0.1877075, \quad (\bar{u}_r)^{II}_{max} = 0.1985936 \quad \rightarrow \quad at \ r = b \ with \ n = 0.1 \ (FIXED - FREE)$

$(\bar{u}_r)^I_{max} = 0.05018 \quad \rightarrow \quad at \ r/b = 0.618 \ with \ n = 0.1 \ (FIXED - FIXED)$

$(\bar{u}_r)^{II}_{max} = 0.05207 \quad \rightarrow \quad at \ r/b = 0.595 \ with \ n = 0.1 \ (FIXED - FIXED)$

As to the maximum radial stress (Figs. 4-6), it is approximately at $r/b \cong 0.4$ under free-free conditions, at the inner surface under fixed-free boundaries, and at the outer surface under fixed-fixed boundary conditions. The maximum radial stress is in compression at fixed-fixed surfaces:

$(\bar{\sigma}_r)^I_{max} = 0.32585 \quad \rightarrow \quad at \ r/b = 0.393 \ with \ n = 0.1 \ (FREE - FREE)$

$(\bar{\sigma}_r)^{II}_{max} = 0.30113 \quad \rightarrow \quad at \ r/b = 0.415 \ with \ n = 0.1 \ (FREE - FREE)$

$(\bar{\sigma}_r)^I_{max} = 0.4797, \quad (\bar{\sigma}_r)^{II}_{max} = 0.383458 \quad \rightarrow \quad at \ r = a \ with \ n = 0.1 \ (FIXED - FREE)$

$(\bar{\sigma}_r)^I_{max} = -0.3232780, \quad (\bar{\sigma}_r)^{II}_{max} = -0.3229234 \quad \rightarrow \quad at \ r = b \ with \ n = 0.1 \ (FIXED - FIXED)$

From the above, a major difference between the two models is observed in the maximum radial stress at the inner surface for $n = 0.1$.

Let's now consider the maximum tangential stresses (Figs. 4-6). It is located immediately before or at just the inner surface under free-free boundary conditions, and at around mid-surface under both fixed-free (at $r/b \cong 0.5$) and fixed-fixed (at $r/b \cong 0.3$) conditions:

$(\bar{\sigma}_\theta)^I_{max} = 0.59 \quad \rightarrow \quad at \ r/b = 0.122 \ with \ n = 0.1 \ (FREE - FREE)$

$(\bar{\sigma}_\theta)^{II}_{max} = 0.58 \quad \rightarrow \quad at \ r = a \ with \ n = 0.1 \ (FREE - FREE)$

$(\bar{\sigma}_\theta)^I_{max} = 0.397 \quad \rightarrow \quad at \ r/b = 0.46 \ with \ n = 0.1 \ (FIXED - FREE)$

$(\bar{\sigma}_\theta)^{II}_{max} = 0.400 \quad \rightarrow \quad at \ r/b = 0.483 \ with \ n = 0.1 \ (FIXED - FREE)$

$(\bar{\sigma}_\theta)^I_{max} = 0.161, \quad (\bar{\sigma}_\theta)^{II}_{max} = 0.155 \quad \rightarrow \quad at \ r/b = 0.325 \ with \ n = 0.1 \ (FIXED - FIXED)$
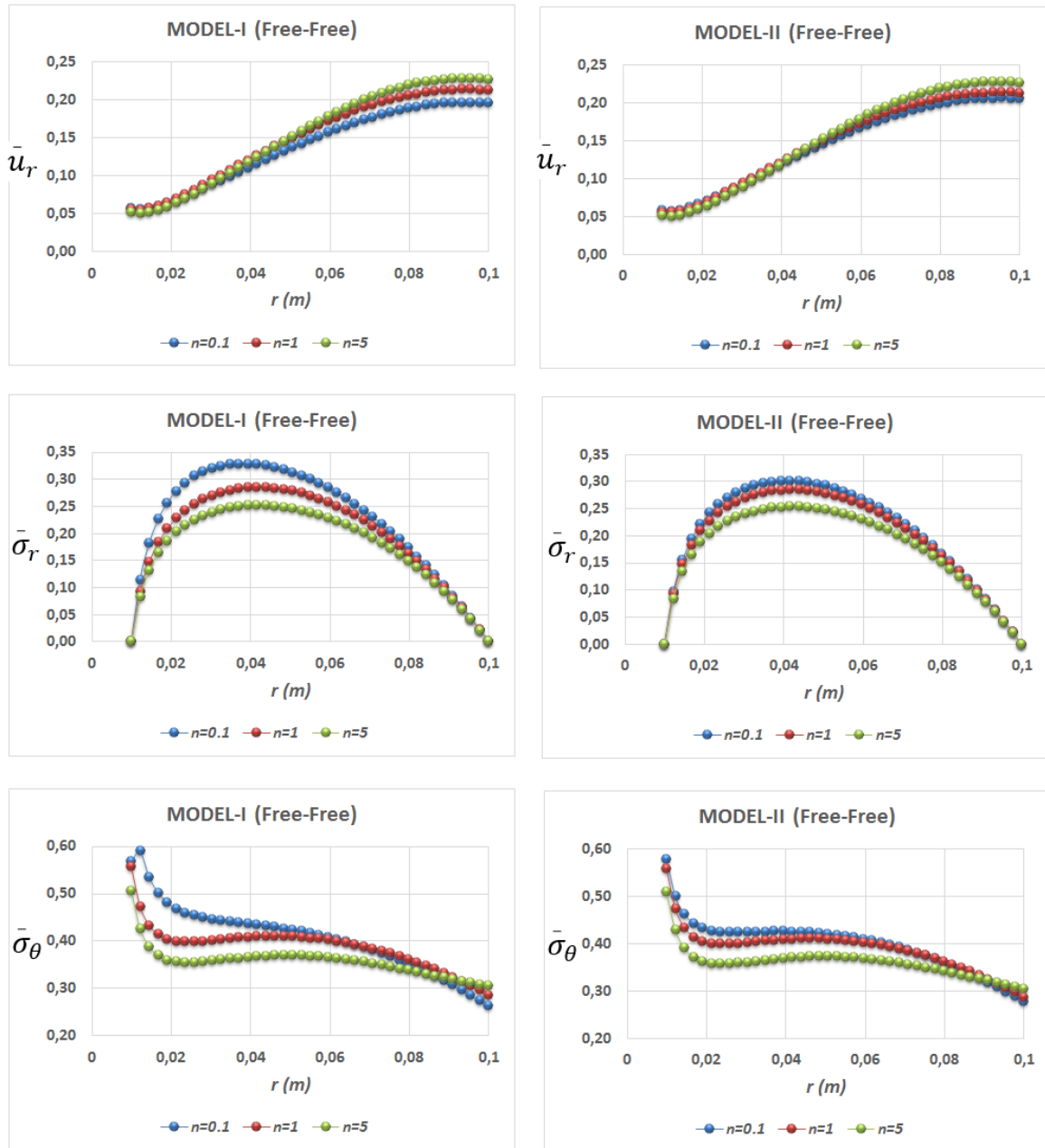
Fig. 4. Dimensionless elastic fields under free-free boundary conditions
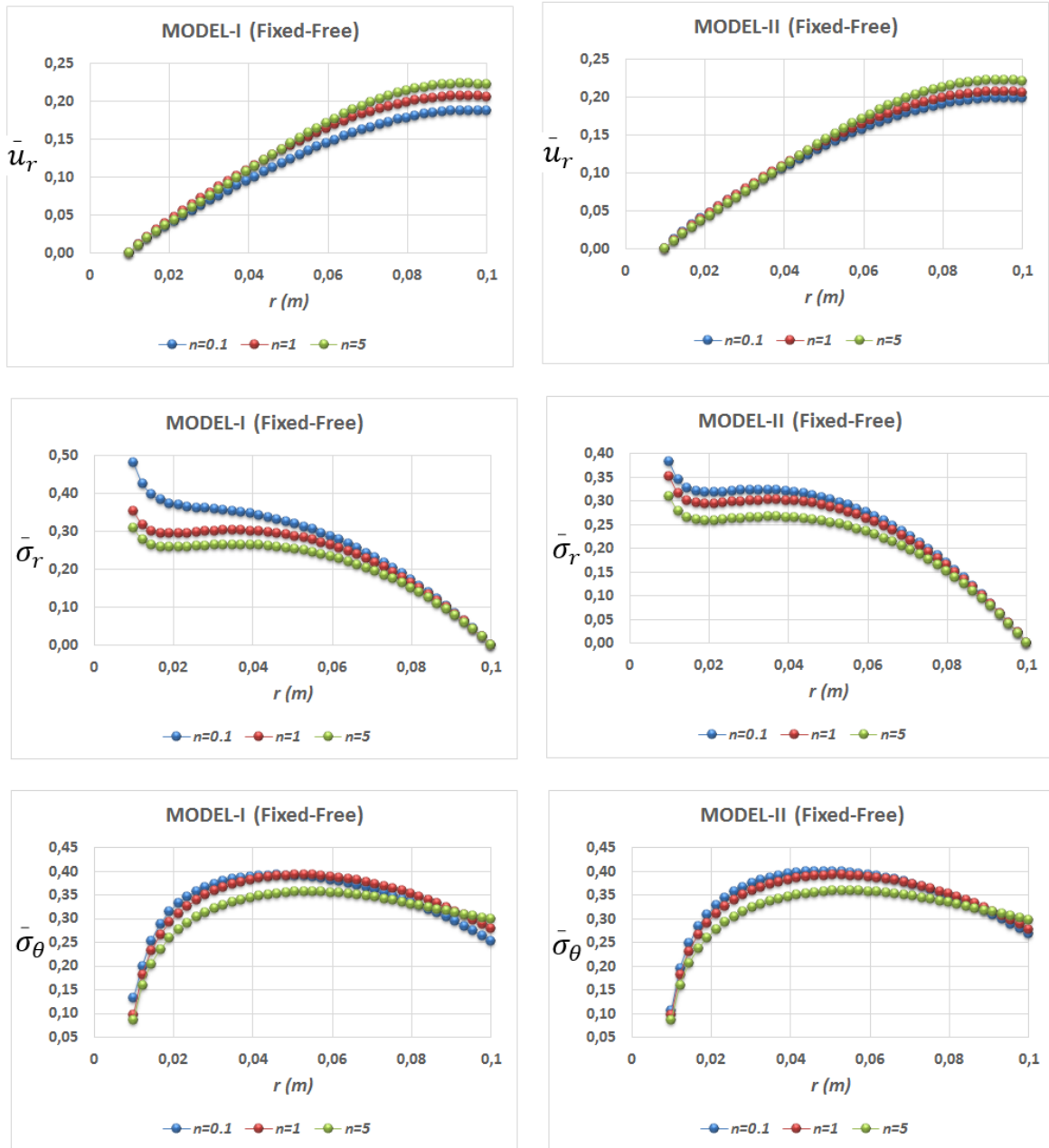
Fig. 5. Dimensionless elastic fields under fixed-free boundary conditions
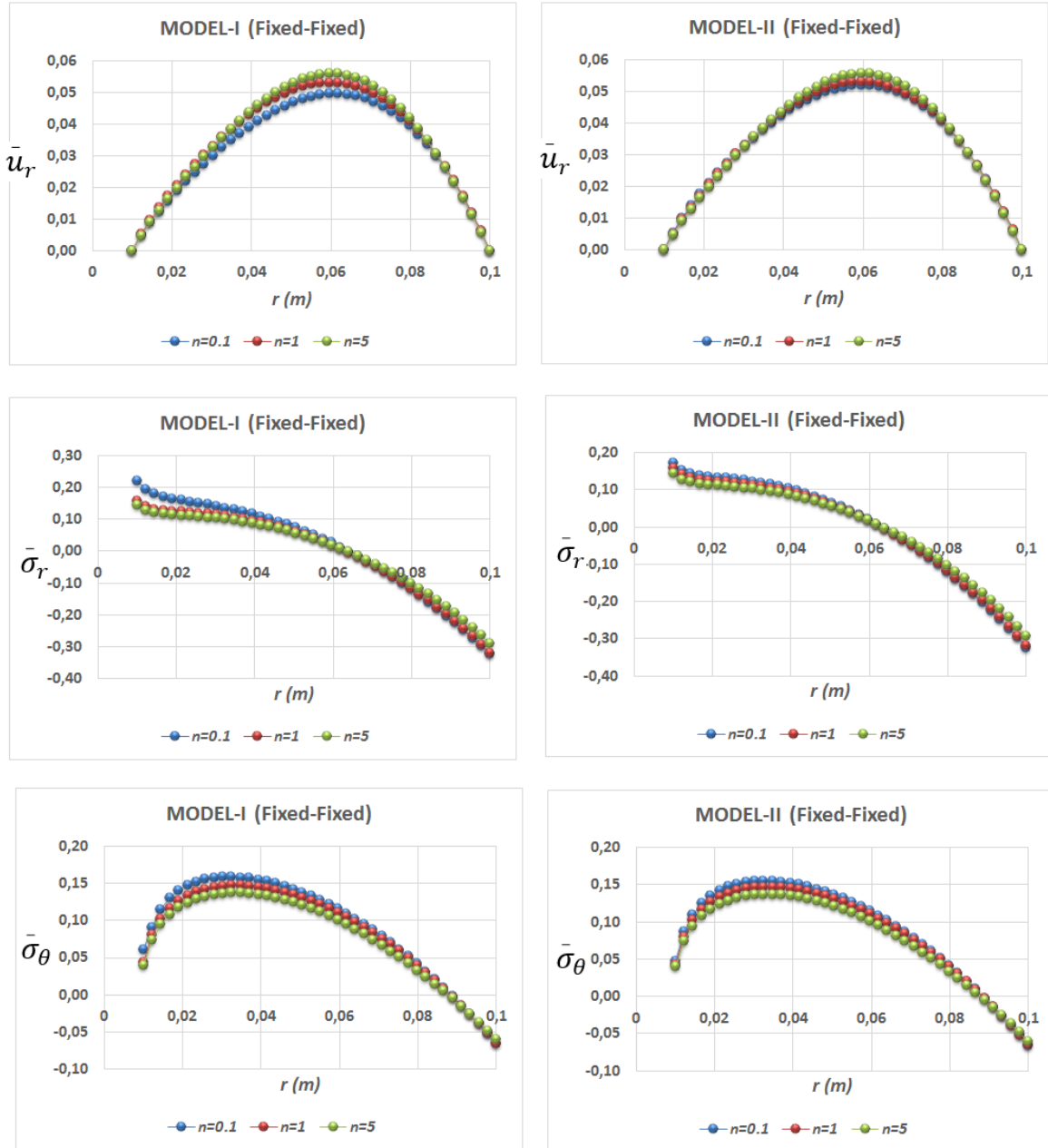
Fig. 6. Dimensionless elastic fields under fixed-fixed boundary conditions

The maximum equivalent stress is located at the inner surface under free-free boundary conditions while it is at the outer surface for fixed-fixed ones (Fig. 7). From Fig. 7, a clear difference between the two models is observed in the value and location of the maximum equivalent stress under fixed-free boundary conditions.

$$(\bar{\sigma}_{eq})^I_{max} = 0.4291, \quad (\bar{\sigma}_{eq})^{II} = 0.3430 \quad \rightarrow \quad at\ r = a\ with\ n = 0.1\ (FIXED - FREE)$$

$$(\bar{\sigma}_{eq})^{II}_{max} = 0.3645\ , (\bar{\sigma}_{eq})^I = 0.37 \quad \rightarrow \quad at\ r/b = 0.438\ with\ n = 0.1\ (FIXED - FREE)$$

Table 3. Comparisons of the transfer matrix method (TMM) and the complementary functions method (CFM) elastic fields in the exponential disk based on the Model-I (n=3)

$r(m)$	$\bar{u}_r$		$\bar{\sigma}_r$		$\bar{\sigma}_\theta$		$\bar{\sigma}_{eq}$	
	CFM	TMM	CFM	TMM	CFM	TMM	CFM	TMM
					Free-Free			
0.01	0.05174	0.05174	0.00000	0.00000	0.51742	0.51742	0.51742	0.51742
0.019	0.05994	0.05994	0.19084	0.19082	0.36828	0.36823	0.31901	0.31897
0.028	0.08367	0.08366	0.23928	0.23925	0.36548	0.36543	0.32152	0.32148
0.037	0.11157	0.11156	0.25696	0.25692	0.37444	0.37440	0.33169	0.33165
0.046	0.13999	0.13997	0.25840	0.25836	0.38041	0.38036	0.33643	0.33638
0.055	0.16659	0.16657	0.24710	0.24706	0.38065	0.38060	0.33451	0.33446
0.064	0.18955	0.18953	0.22391	0.22387	0.37490	0.37485	0.32671	0.32667
0.073	0.20747	0.20744	0.18866	0.18862	0.36362	0.36357	0.31498	0.31493
0.082	0.21942	0.21939	0.14055	0.14051	0.34742	0.34738	0.30270	0.30267
0.091	0.22494	0.22493	0.07827	0.07825	0.32679	0.32676	0.29553	0.29551
0.1	0.22399	0.22399	0.00000	0.00000	0.30183	0.30183	0.30183	0.30183
					Fixed-Free			
0.01	0.00000	0.00000	0.31646	0.31646	0.08738	0.08738	0.28308	0.28307
0.019	0.03653	0.03653	0.26398	0.26400	0.26518	0.26521	0.26459	0.26460
0.028	0.06899	0.06899	0.26941	0.26942	0.32118	0.32120	0.29867	0.29870
0.037	0.10094	0.10095	0.27276	0.27278	0.34975	0.34978	0.31831	0.31834
0.046	0.13161	0.13162	0.26778	0.26780	0.36430	0.36433	0.32691	0.32693
0.055	0.15958	0.15959	0.25304	0.25306	0.36889	0.36892	0.32675	0.32678
0.064	0.18340	0.18341	0.22776	0.22778	0.36554	0.36557	0.31975	0.31978
0.073	0.20187	0.20189	0.19110	0.19113	0.35563	0.35566	0.30827	0.30830
0.082	0.21418	0.21419	0.14198	0.14200	0.34022	0.34025	0.29598	0.29600
0.091	0.21992	0.21993	0.07892	0.07893	0.32001	0.32003	0.28876	0.28877
0.1	0.21910	0.21910	0.00000	0.00000	0.29523	0.29523	0.29523	0.29523
					Fixed-Fixed			
0.01	0.00000	0.00000	0.14401	0.14401	0.03976	0.03976	0.12882	0.12882
0.019	0.01622	0.01622	0.11362	0.11363	0.11676	0.11677	0.11522	0.11523
0.028	0.02946	0.02946	0.10540	0.10541	0.13450	0.13451	0.12257	0.12258
0.037	0.04080	0.04080	0.09165	0.09166	0.13630	0.13631	0.12036	0.12037
0.046	0.04938	0.04939	0.06926	0.06927	0.12832	0.12833	0.11124	0.11125
0.055	0.05415	0.05415	0.03727	0.03728	0.11247	0.11248	0.09923	0.09924
0.064	0.05420	0.05420	-0.0051	-0.0051	0.08975	0.08976	0.09240	0.09241
0.073	0.04891	0.04892	-0.0588	-0.0588	0.06080	0.06081	0.10356	0.10356
0.082	0.03803	0.03804	-0.1250	-0.1250	0.02596	0.02597	0.13980	0.13980
0.091	0.02163	0.02163	-0.2054	-0.2054	-0.0148	-0.0148	0.19843	0.19842
0.1	0.00000	0.00000	-0.3021	-0.3021	-0.0619	-0.0619	0.27637	0.27637

Table 4. Comparisons of the transfer matrix method (TMM) and the complementary functions method (CFM) elastic fields in the exponential disk based on the Model-II (n=3)

$r(m)$	$\bar{u}_r$		$\bar{\sigma}_r$		$\bar{\sigma}_\theta$		$\bar{\sigma}_{eq}$	
	CFM	TMM	CFM	TMM	CFM	TMM	CFM	TMM
				Free-Free				
0.01	0.05218	0.05218	0.00000	0.00000	0.52180	0.52180	0.52180	0.52180
0.019	0.06044	0.06043	0.19264	0.19262	0.37178	0.37173	0.32204	0.32200
0.028	0.08422	0.08421	0.24170	0.24167	0.36908	0.36904	0.32470	0.32466
0.037	0.11202	0.11200	0.25967	0.25964	0.37807	0.37803	0.33495	0.33491
0.046	0.14014	0.14012	0.26116	0.26112	0.38395	0.38390	0.33963	0.33958
0.055	0.16631	0.16629	0.24968	0.24963	0.38400	0.38395	0.33752	0.33747
0.064	0.18881	0.18879	0.22610	0.22606	0.37794	0.37789	0.32941	0.32936
0.073	0.20637	0.20635	0.19029	0.19025	0.36613	0.36608	0.31716	0.31712
0.082	0.21812	0.21810	0.14153	0.14150	0.34904	0.34900	0.30407	0.30404
0.091	0.22360	0.22358	0.07865	0.07862	0.32700	0.32697	0.29563	0.29561
0.1	0.22267	0.22267	0.00000	0.00000	0.30005	0.30005	0.30005	0.30005
				Fixed-Free				
0.01	0.00000	0.00000	0.31979	0.31979	0.08830	0.08830	0.28605	0.28605
0.019	0.03686	0.03687	0.26684	0.26686	0.26788	0.26791	0.26737	0.26738
0.028	0.06945	0.06946	0.27240	0.27242	0.32434	0.32436	0.30174	0.30176
0.037	0.10132	0.10133	0.27583	0.27585	0.35302	0.35305	0.32145	0.32148
0.046	0.13169	0.13170	0.27077	0.27079	0.36751	0.36754	0.32996	0.32998
0.055	0.15923	0.15924	0.25577	0.25580	0.37194	0.37197	0.32959	0.32962
0.064	0.18259	0.18260	0.23005	0.23007	0.36831	0.36834	0.32225	0.32228
0.073	0.20070	0.20072	0.19280	0.19282	0.35791	0.35794	0.31027	0.31029
0.082	0.21281	0.21282	0.14300	0.14302	0.34165	0.34167	0.29718	0.29720
0.091	0.21850	0.21851	0.07930	0.07931	0.32007	0.32009	0.28871	0.28872
0.1	0.21770	0.21770	0.00000	0.00000	0.29335	0.29335	0.29335	0.29335
				Fixed-Fixed				
0.01	0.00000	0.00000	0.14493	0.14493	0.04002	0.04002	0.12964	0.12964
0.019	0.01630	0.01630	0.11440	0.11440	0.11748	0.11749	0.11597	0.11598
0.028	0.02955	0.02955	0.10617	0.10618	0.13532	0.13533	0.12336	0.12337
0.037	0.04082	0.04082	0.09234	0.09235	0.13714	0.13716	0.12113	0.12114
0.046	0.04928	0.04929	0.06976	0.06977	0.12918	0.12919	0.11199	0.11200
0.055	0.05395	0.05395	0.03743	0.03744	0.11336	0.11337	0.10004	0.10005
0.064	0.05397	0.05397	-0.0054	-0.0054	0.09064	0.09065	0.09346	0.09347
0.073	0.04875	0.04875	-0.0597	-0.0597	0.06159	0.06160	0.10504	0.10504
0.082	0.03800	0.03800	-0.1266	-0.1266	0.02649	0.02650	0.14167	0.14167
0.091	0.02169	0.02169	-0.2075	-0.2075	-0.0147	-0.0147	0.20054	0.20054
0.1	0.00000	0.00000	-0.3043	-0.3043	-0.0623	-0.0623	0.27846	0.27846

Finally, Table 3 and 4 reveals that the results obtained by both methods overlap. Very minor differences between TMM and CFM solutions (the maximal relative error for the equivalent stress is about 10^{-4} for Model-I) may probably stem from the numerical integration technique used in TMM together with the FG orthotropic nature of the disk material and geometry. For example, when a uniform disk with power-law graded of a single orthotropic material is considered, two solution methods have been presented the same results to the seven digits after dot with the analytical solutions [61]. The maximum degree of precision numerical integration technique has been used in the present study in TMM. RK4 has been employed in CFM

solutions. When necessary, with the help of the properties of the transfer matrix method, it is also possible to increase the accuracy of the homogeneous and particular solutions without changing the accuracy of Runge-Kutta and numerical integration techniques.

6. Discussion

The complementary functions method (CFM) is one of the techniques in IVP solvers. It may be used directly or as an assistant tool as in the present study for solving some kinds of problems. The main feature of the problems to be directly handled by CFM is that there must not be any intermediate singular loads in the domain considered. For instance, the bending of a beam subjected to a singular force cannot be directly studied by CFM. To exemplify, concentric disks without the residual internal stresses may be studied by CFM by letting larger matrix dimensions. In these cases, both CPU time and the volume of the computer code also increase extremely.

The transfer matrix method (TMM) is a more general solution method than CFM. Many complex problems may be considered by TMM. For example, concentric disks may be studied by TMM without increasing the size of matrices and also considering the residual internal stresses at the intermediate contact surfaces of the disks. Due to these reasons, and to build a foundation for such kinds of advanced problems [77-81], the transfer matrix method solution technique in which the transfer matrix has been obtained with the help of CFM is preferred in this study.

In the method of CFM, the general solution of BVP in Eq. (4) reads [49]

$$u_r(r) = u_r^{(0)}(r) + b_1 u_r^{(1)}(r) + b_2 u_r^{(2)}(r) \tag{18}$$

Where $u_r^{(1)}(r)$ and $u_r^{(2)}(r)$ characterize the homogeneous solutions of Eq. (4) under prescribed Kronecker delta initial conditions ($u_r(a)=1$ and $du_r(r)/dr|_{r=a}=0$ for the determination of $u_r^{(1)}(r)$; and $u_r(a)=0$ and $du_r(r)/dr|_{r=a}=1$ for the determination of $u_r^{(2)}(r)$) while $u_r^{(0)}(r)$ is the nonhomogeneous solutions of Eq. (4) under zero initial conditions ($u_r(a)=0$ and $du_r(r)/dr|_{r=a}=0$); b_1, and b_2 are the other unknowns which are determined by plugging the physical boundary conditions in the solution (18). CFM solutions for both the radial displacement and the radial stress may be written in a compact form as

$$\begin{Bmatrix} u_r(r) \\ \sigma_r(r) \end{Bmatrix} = \begin{bmatrix} u_r^{(1)}(r) & u_r^{(2)}(r) \\ \sigma_r^{(1)}(r) & \sigma_r^{(2)}(r) \end{bmatrix} \begin{Bmatrix} b_1 \\ b_2 \end{Bmatrix} + \begin{Bmatrix} u_r^{(0)}(r) \\ \sigma_r^{(0)}(r) \end{Bmatrix} \tag{19}$$

Yıldırım [49] also showed that the CFM solution inherently covers the fundamental matrix or the transfer matrix by an alias, as follows

$$\boldsymbol{F}(a,r) = \begin{bmatrix} u_r^{(1)}(r) & u_r^{(2)}(r) \\ \sigma_r^{(1)}(r) & \sigma_r^{(2)}(r) \end{bmatrix} \begin{bmatrix} u_r^{(1)}(a) & u_r^{(2)}(a) \\ \sigma_r^{(1)}(a) & \sigma_r^{(2)}(a) \end{bmatrix}^{-1} \tag{20}$$

As stated above, the accuracy of the numerical results strictly depends on the accuracy of the numerical transfer matrix. Both the material orthotropy [61] and the thickness gradient [49]

significantly influence the accuracy of the transfer matrix. After the determination of the elements of the transfer matrix with a desired accuracy within the acceptable engineering errors, the solution is obtained by employing Eq. (8) in the transfer matrix method (see Appendix).

In practice, a small part of the radial coordinate may be graded. The whole disk may compose of several disks with different profiles. The residual internal stresses due to the shrinking process including hub and blade pressures should be included in the analysis. As stated above, the transfer matrix method is to be a very useful choice for the solution of such types of problems. The author aims to step-by-step study more advanced problems based on the well-founded analytical and numerical results.

7. Conclusions

Minimizing weight and maximizing strength in gas turbine discs in the aerospace industry, such as turbojet engines, are the main practical applications of functionally graded and rotating discs of varying thickness. Since there is no single FG-material type or thickness variation function that can be a recipe for all kinds of problems, different thickness functions (linear, exponential, hyperbolic, parabolic, etc.) and basic properties of FG-material components (isotropic, orthotropic, etc.) are currently studied in the existing literature. Contrary to producing inhomogeneous material from two isotropic materials, unfortunately, the number of studies based on inhomogeneous material from two orthotropic materials is not yet sufficient as the problem becomes more complex. One of the main aims of this study is to fill this gap to some extent with numerical solutions having acceptable precision.

The problem chosen involves an elastic analysis of exponentially varying thickness rotating disks under three boundary conditions. Two orthotropic materials are graded based on a simple Voigt mixture rule with powers of volume fraction of constituents as the disk inhomogeneous and orthotropic material. Two models are used in the volume fraction of constituents. Results are tabulated and illustrated in graphical forms. There are no such significant differences in CPU-time and accuracy in the solutions by the two methods for the proposed example in which the disk consists of a single body having continuously varying material and thickness properties.

Previous studies showed that decreasing thickness profiles from the inner surface towards the outer propose more suitable stress distributions than the uniform ones under centrifugal forces. Another scope of the present study is to have a comparison of two Voigt grading models for the same disk thickness profile. For the chosen material and disk profile whose thickness smoothly decreases from the inner surface towards the outer, in general, such remarkable differences are not observed between the results of the two material grading models for $n > 1$. They may be much more noticeable when different profiles and different orthotropic materials having different orthotropy degrees are used. Besides, if Model-I is used, the choice of inhomogeneity indexes, which are equal to or greater than 0.5, may be recommended.
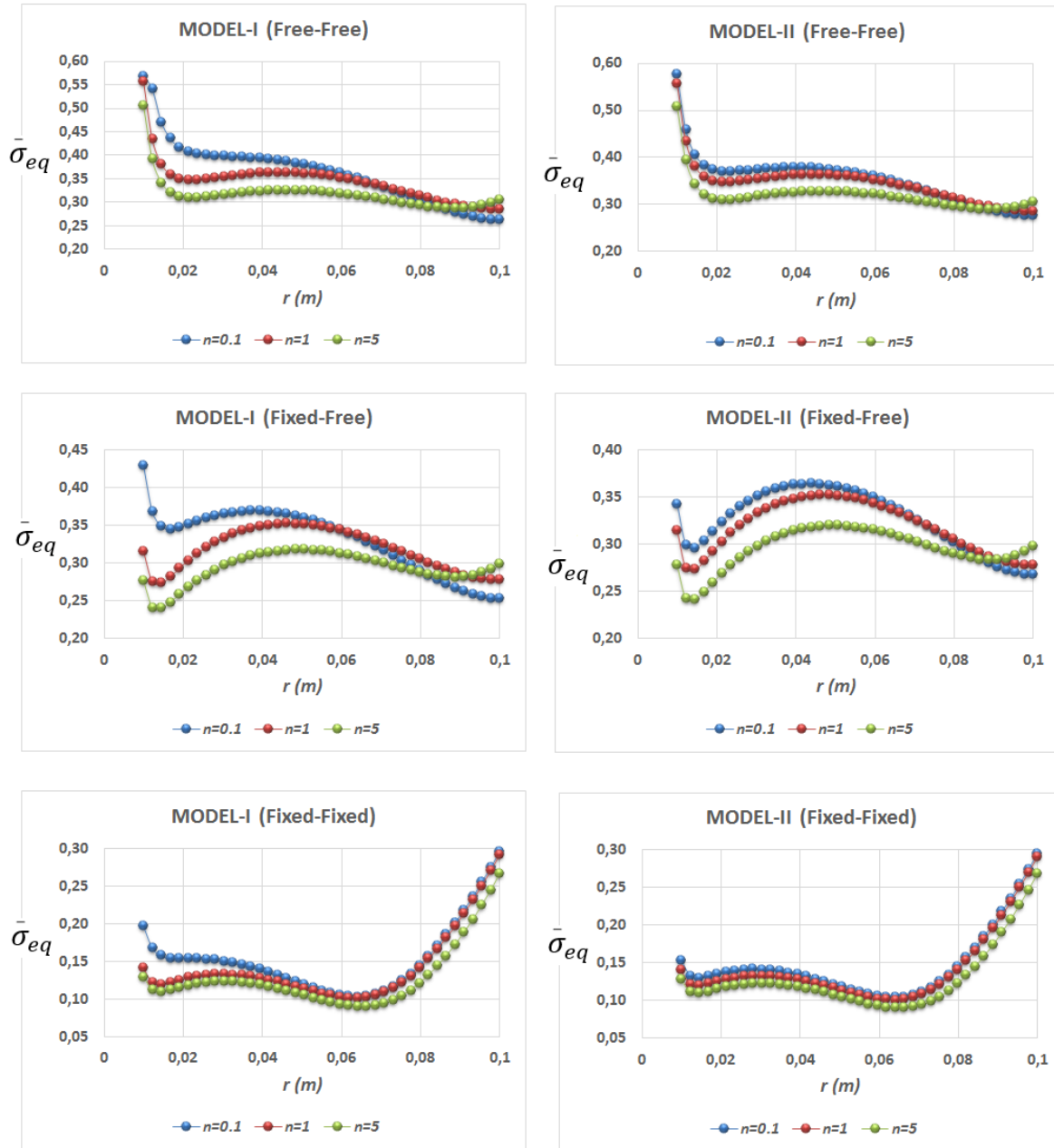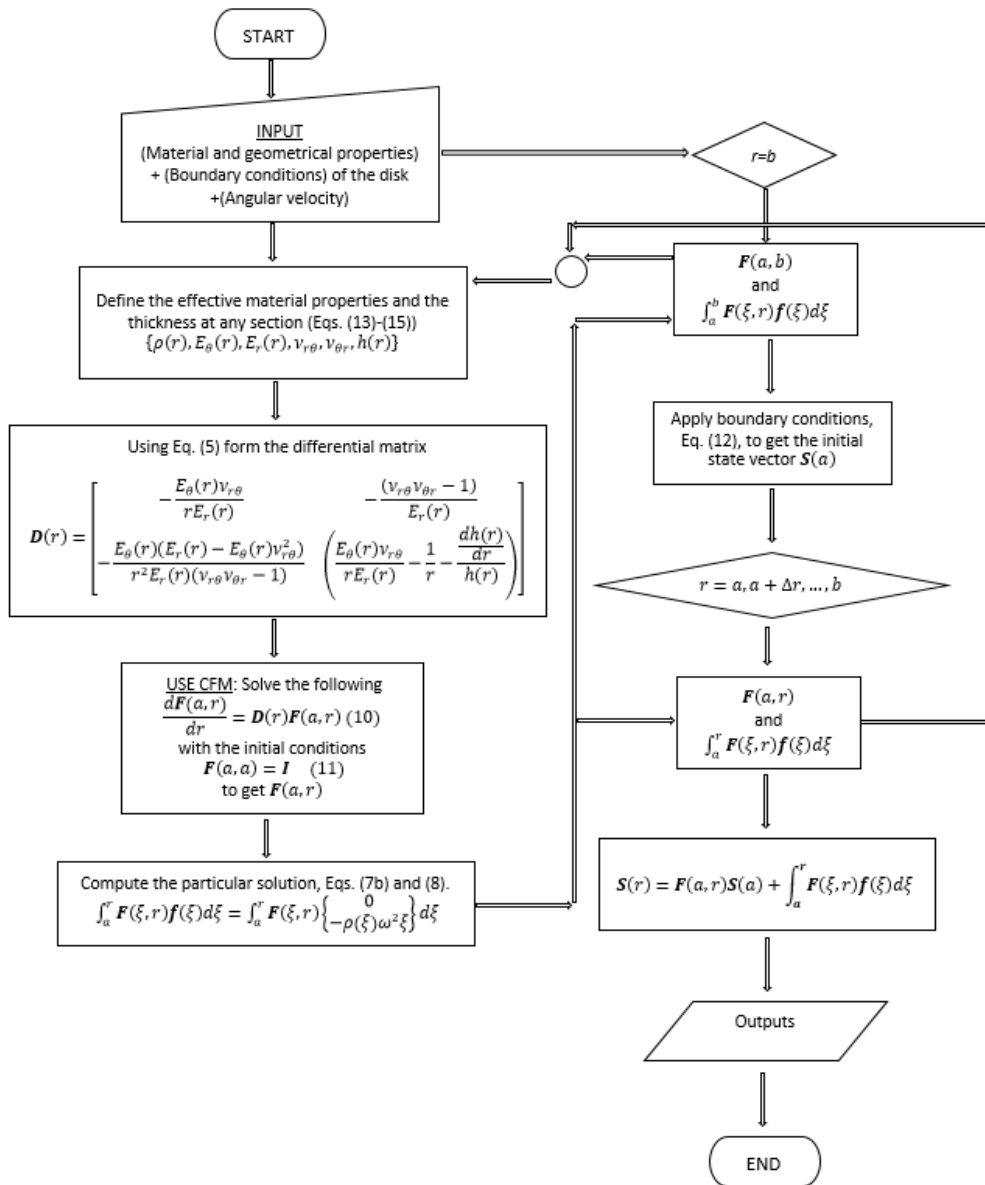
31

Fig. 7. Dimensionless equivalent stresses under three boundary conditions based on the two models.

Appendix: Flowchart of TMM procedure

Declaration of Conflicting Interests

Acknowledgement

Notations

a, b	Inner and outer radii of the disk
C_{ij} ($i = 1,2$ and $j = 1,2$)	Transformed on-axis in-plane stiffness terms
D	Differential matrix
E_r, E_θ	Anisotropic Young's moduli
f	Nonhomogeneous vector
F	Transfer matrix
h	thickness
I	Unit matrix
k, m	Constants for the disk profile
n	Inhomogeneity index
r, θ	Radial and circumferential coordinates
S	State vector
u_r	Radial displacement
V_A, V_B	Volume fractions of Materials A and B
ω	Angular velocity
$\varepsilon_r, \varepsilon_\theta$	Radial and circumferential strains
$\nu_{r\theta}, \nu_{\theta r}$	Anisotropic Poisson's ratios
ρ	Material density
σ_{eq}	Von-Mises equivalent stress
σ_r, σ_θ	Radial and circumferential stresses

References

[1] Tang S. Elastic stresses in rotating anisotropic discs. *Int J Mech Sci* (IJMS), 11, 509–517, 1969.

[2] Murthy D, Sherbourne A. Elastic stresses in anisotropic discs of variable thickness. *Int J Mech Sci,* 12, 627-640, 1970.

[3] Reddy TY, Srinath H. Elastic stresses in a rotating anisotropic annular disc of variable thickness and variable density. *Int J Mech Sci,* 16(2), 85-89, 1974.

[4] Chang CI. A closed-form solution for an orthotropic rotating disc. *J Appl Mech,* 41(4), 1122–1123, 1974.

[5] Chang CI. The anisotropic rotating discs. *Int J Mech Sci* 1975; 17(6): 397-402.

[6] Bert CW. Centrifugal stresses in arbitrarily laminated, rectangular-anisotropic circular discs. *J Strain Anal Eng Des,* 10, 84-92, 1975.

[7] Gurushankar GV. Thermal stresses in a rotating nonhomogeneous, anisotropic disc of varying thickness and density. *J Strain Anal Eng Des,* 10, 137-142, 1975.

[8] Christensen RM, Wu EM. Optimal design of anisotropic (fiber-reinforced) flywheels. *J Compos Mater,* 11, 395-404, 1977.

[9]Belingardi G, Genta G, Gola M. A study of the stress distribution in rotating, orthotropic discs. *Composites,* 10(2), 77-80, 1979.

[10]Genta G, Gola M. The stress distribution in orthotropic rotating discs. *J Appl Mech,* 48, 559-562, 1981.

[11]Jain R, Ramachandra K, Simha KRY. Rotating anisotropic disk of uniform strength. *Int J Mech Sci,* 41, 639–648, 1999.

[12]Tutuncu N. Effect of anisotropy on stresses in rotating discs. *Int J Mech Sci,* 37, 873–881, 2000.

[13]Zhou F, Ogawa A. Elastic solutions for a solid rotating disc with cubic anisotropy. *J Appl Mech,* 69, 81-83, 2002.

[14]Callioglu H. Stress analysis of an orthotropic rotating disc under thermal loading. *J Reinf Plast Compos,* 23(17), 1857–1869, 2004.

[15]Callioglu H, Topcu M, Altan G. Stress analysis of curvilinearly orthotropic rotating discs under mechanical and thermal loading. *J Reinf Plast Compos,* 24, 831-838, 2005.

[16]Sayer M, Topcu M, Bektas NB, Tarakcilar AR. Thermoelastic stress analysis in a thermoplastic composite disc. *Sci Eng Compos Mater,* 12(4), 251–260, 2005.

[17]Tahani M, Nosier A, Zebarjad SM. Deformation and stress analysis of circumferentially fiber-reinforced composite disks. *Int J Solids Struct,* 42(9-10), 2741–2754, 2005.

[18]Zenkour AM, Allam NMN. On the rotating fiber-reinforced viskoelastic composite solid and annular disks of variable thickness. *Int J Comput Methods Eng Sci Mech,* 7, 21-31,2006.

[19]Callioglu H, Topcu M, Tarakçılar AR. Elastic-plastic stress analysis of an orthotropic rotating disc. *Int J Mech Sci,* 48, 985-990, 2006.

[20]Callioglu H. Thermal stress analysis of curvilinearly orthotropic rotating discs. *J Thermoplast Compos Mater,* 20, 357-369, 2007.

[21]Alexandrova N, Vila Real PMM. Deformation and stress analysis of an anisotropic rotating annular disk. *Int J Comput Methods Eng Sci Mech,* 9(1), 43–50, 2008.

[22]Sen F, Koruvatan T, Aldas K, Thermal residual stresses in thermoplastic composite disc with holes using 3D-FEM. *Adv Compos Lett,* 23(4), 79-87, 2014.

[23]Eraslan AN, Kaya Y, Varlı E. Analytical solutions to orthotropic variable thickness disk problems. *Pamukkale University Journal of Engineering Sciences,* 22(1), 24–30, 2016.

[24]Yıldırım V. The complementary functions method (CFM) solution to the elastic analysis of polar orthotropic rotating discs. *Journal of Applied and Computational Mechanics (JACM),* 4(3), 216-230, 2018.   DOI: 10.22055/JACM.2017.23188.1150

[25]Horgan C, Chan A. The pressurized hollow cylinder or disk problem for functionally graded isotropic linearly elastic materials. *J Elasticity,* 55, 43-59, 1999.

[26]Horgan C, Chan A. The stress response of functionally graded isotropic linearly elastic rotating disks. *J Elasticity,* 55, 219-230, 1999.

[27]Zenkour AM. Analytical solutions for rotating exponentially-graded annular disks with various boundary conditions. *Int J Struct Stab Dy,* 5, 557-577, 2005.

[28]Eraslan AN, Akiş T. On the plane strain and plane stress solutions of functionally graded rotating solid shaft and solid disk problems. *Acta Mechanica,* 181(1–2), 43–63, 2006.

[29]Zenkour AM. Elastic deformation of the rotating functionally graded annular disk with rigid casing. *J Mater Sci,* 42, 9717-9724, 2007.

[30]You LH, You XY, Zhang JJ, Li J. On rotating circular disks with varying material properties. *Zeitschrift für angewandte Mathematik und Physik ZAMP,* 58, 1068–1084, 2007.

[31]Bayat M, Saleem M, Sahari B, Hamouda A, Mahdi E. Analysis of functionally graded rotating disks with variable thickness. *Mech Res Commun,* 35, 283-309, 2008.

[32]Vivio F, Vullo V. Elastic stress analysis of rotating converging conical disks subjected to thermal load and having variable density along the radius. *Int J Solids Struct,* 44, 7767–7784, 2007.

[33]Vullo V, Vivio F. Elastic stress analysis of non-linear variable thickness rotating disks subjected to thermal load and having variable density along the radius. *Int J Solids Struct,* 45, 5337–5355, 2008.

[34]Hojjati MH, Jafari. S Semi exact solution of elastic non uniform thickness and density rotating disks by Homotopy Perturbation and Adomian's decomposition methods Part I: Elastic solution. *Int J Pres Ves Pip,* 85, 871-878, 2008.

[35] Hojjati MH, Hassani A. Theoretical and numerical analyses of rotating discs of nonuniform thickness and density. *Int J Pres Ves Pip,* 85, 694-700, 2008.

[36]Nie GJ, Batra RC. Stress analysis and material tailoring in isotropic linear thermoelastic incompressible functionally graded rotating disks of variable thickness. *Compos Struct,* 92, 720-729, 2010.

[37]Çallıoğlu H, Bektaş NB, Sayer M. Stress analysis of functionally graded rotating discs: Analytical and numerical solutions. *Acta Mech Sinica,* 27, 950-955, 2011.

[38]Hassani A, Hojjati MH, Farrahi G, Alashti RA. Semi-exact elastic solutions for thermomechanical analysis of functionally graded rotating disks. *Compos Struct,* 93, 3239-3251, 2011.

[39]Zenkour AM, Mashat DS. Stress function of a rotating variable-thickness annular disk using exact and numerical methods. *Engineering,* 3, 422-430, 2011.

[40]Argeso H. Analytical solutions to variable thickness and variable material property rotating disks for a new three-parameter variation function. *Mech Based Des Struc,* 40, 133-152, 2012.

[41] Nejad MZ, Abedi M, Lotfian MH, Ghannad M. Elastic analysis of exponential FGM disks subjected to internal and external pressure. *Central European Journal of Engineering,* 3, 459-465, 2013.

[42] Nejad MZ, Rastgoo A, Hadi A. Exact elasto-plastic analysis of rotating disks made of functionally graded materials. *Int J Eng Sci,* 85, 47-57, 2014.

[43] Eraslan AN, Arslan E. Analytical and numerical solutions to a rotating FGM disk. *Journal of Multidisciplinary Engineering Science and Technology (JMEST),* 2(10), 2843-2850, 2015.

[44] Yıldırım V. Analytic solutions to power-law graded hyperbolic rotating discs subjected to different boundary conditions. *International Journal of Engineering & Applied Sciences (IJEAS),* 8(1), 38-52, 2016.

[45] Yıldırım V, Kacar İ. Introducing a computer package program for elastic analysis of functionally graded rotating thick-walled annular structures. *Digital Proceeding of ICOCEE – Cappadocia 2017, S. Sahinkaya and E. Kalıpcı (Editors), Nevsehir, TURKEY, May 8-10,* 1733-1742, 2017.

[46] Yıldırım V. Effects of inhomogeneity and thickness parameters on the elastic response of a pressurized hyperbolic annulus/disc made of functionally graded material. *International Journal of Engineering & Applied Sciences (IJEAS),* 9(3), 36-50, 2017. DOI: 10.24107/ijeas.329433

[47] Gang M. Stress analysis of variable thickness rotating FG disc. *International Journal of Pure and Applied Physics,* 13(1), 158-161, 2017.

[48] Yıldırım V. A parametric study on the centrifugal force-induced stress and displacements in power-law graded hyperbolic discs. *Lati Am J Solids Stru (LAJSS),* 15(4), 1-16, 2018.

[49] Yıldırım V. Numerical elasticity solution for continuously tapered and arbitrarily functionally graded (FG) rotating disks via the transfer matrix approach. *International Journal of Mathematics and Computational Science,* 4(2), 48-73, 2018.

[50] Khorsand M, Tang Y. Design functionally graded rotating disks under thermoelastic loads: Weight optimization. *Int J Pres Ves Pip,* 161, 33–40, 2018.

[51] Durodola J, Attia O. Deformation and stresses in functionally graded rotating discs. *Compos Sci Technol,* 60, 987-995, 2000.

[52] Chen J, Ding H, Chen W. Three-dimensional analytical solution for a rotating disc of functionally graded materials with transverse isotropy. *Archive of Applied Mechanics,* 77, 241-251, 2007.

[53] Nie GJ, Zhong Z, Batra RC. Material tailoring for orthotropic rotating disks. *Compos Sci Technol,* 71, 406-414, 2011.

[54] Kansal G, Parvez M. Thermal stress analysis of orthotropic graded rotating discs. *International Journal of Modern Engineering Research (IJMER),* 2(5), 3881-3885, 2012.

[55] Lubarda VA. On pressurized curvilinearly orthotropic circular disc, cylinder and sphere made of radially nonuniform material. *J Elasticity,* 109, 103-133, 2012.

[56] Peng XL, Li XF. Elastic analysis of rotating functionally graded polar orthotropic discs. *Int J Mech Sci (IJMS),* 60, 84-91, 2012.

[57] Kacar I, Yıldırım V. Effect of the anisotropy ratios on the exact elastic behavior of functionally power-graded polar orthotropic rotating uniform discs under various boundary conditions. *Digital Proceeding of ICOCEE – Cappadocia 2017, Nevsehir, Turkey,* 1743-1752, 2017.

[58] Essa S, Argeso H. Elastic analysis of variable profile and polar orthotropic FGM rotating disks for a variation function with three parameters. *Acta Mechanica,* 228, 3877–3899,2017.

[59] Zheng Y, Bahaloo H, Mousanezhad D, Vaziri A, Nayeb-Hashemi H. Displacement and stress fields in a functionally graded fiber-reinforced rotating disk with nonuniform thickness and variable angular velocity. *J Eng Mater-T ASME,* 39, 031010-1-9, 2017.

[60] Yıldırım V. Unified exact solutions to the hyperbolically tapered pressurized/rotating disks made of nonhomogeneous isotropic/orthotropic materials. *International Journal of Advanced Materials Research,* 4(1), 1-23, 2018.

[61] Yıldırım V. Numerical/analytical solutions to the elastic response of arbitrarily functionally graded polar orthotropic rotating discs. *J Braz Soc Mech Sci & Eng,* 40, 1-21, 2018.

[62] İnan M. *The Method of Initial Values and the Carry-Over Matrix in Elastomechanics.* ODTÜ M., Publication, Ankara, No: 20, 1968.

[63] Haktanır V, Kiral E. Statical analysis of elastically and continuously supported helicoidal structures by the transfer and stiffness matrix methods. *Computers and Structures,* 49(4), 663-677, 1993.

[64] Chen YZ, Lin XY. An alternative numerical solution of thick-walled cylinders and spheres made of functionally graded materials. *Comp Mater Sci,* 48, 640–647, 2010.

[65] Arici M, Granata MF. Generalized curved beam on elastic foundation solved by Transfer Matrix Method. *Structural Engineering & Mechanics,* 40(2), 279-295, 2011.

[66] Garus S, Sochacki W. One dimensional phononic FDTD algorithm and transfer matrix method implementation for severin aperiodic multilayer. *Journal of Applied Mathematics and Computational Mechanics,* 16(4), 17-27, 2017.

[67] Wimmer H, Nachbagauer K. Exact transfer- and stiffness matrix for the composite beam-column with refined zigzag kinematics. *Compos Struct,* 189, 700-706, 2018.

[68] Zhong H, Liu Z, Qin H, Liu Y. Static analysis of thin-walled space frame structures with arbitrary closed cross-sections using transfer matrix method. *Thin Wall Struct,* 123, 255-269, 2018.

[69] Yıldırım V. Several stress resultant and deflection formulas for Euler-Bernoulli beams under concentrated and generalized power/sinusoidal distributed loads. *International*

Journal of Engineering & Applied Sciences (IJEAS), 10(2), 35-632018. DOI: 10.24107/ijeas.430666

[70]Aktas Z. *Numerical Solutions of Two-Point Boundary Value Problems*. Ankara, Turkey, METU, Dept of Computer Eng, 1972.

[71]Roberts S, Shipman J. Fundamental matrix and two-point boundary-value problems. *J Optimiz Theory App,* 28(1), 77-88, 1979.

[72]Haktanir V, Kıral E. Direct application of complementary functions method to axisymmetrical shells and cylindrical vaults (barrels). *Journal of Isparta Eng Faculty of Akdeniz Un.*, 6, 220-239, 1991.

[73]Haktanır V. The complementary functions method for the element stiffness matrix of arbitrary spatial bars of helicoidal axes. *Int J Numer Meth Eng,* 38(6), 1031–1056, 1995. Doi:10.1002/nme.1620380611

[74]Yıldırım V. Free vibration analysis of non-cylindrical coil springs by combined use of the transfer matrix and the complementary functions methods. *Commun Numer Meth Eng,* 13(6), 487–494, 1997.

[75]Yıldırım V. A parametric study on the natural frequencies of unidirectional composite conical springs. *Commun Numer Meth Eng,* 20(3), 207–227, 2004.

[76]Eraslan AN, Orcan Y. Elastic–plastic deformation of a rotating solid disk of exponentially varying thickness. *Mech Mater,* 34, 423-432, 2002.

[77] Yıldırım, V. The best grading pattern selection for the axisymmetric elastic response of pressurized inhomogeneous annular structures (sphere/ cylinder/annulus) including rotation. Journal of the Brazilian Society of Mechanical Sciences and Engineering. 42:109, 2020. https://doi.org/10.1007/s40430-020-2193-x

[78]Avcar M., Hadji L., Civalek Ö. Natural frequency analysis of sigmoid functionally graded sandwich beams in the framework of high order shear deformation theory. *Composite Structures*, 276, 114564, 2021. https://doi.org/10.1016/j.compstruct.2021.114564.

[79]Hadji L., Avcar M., Zouatnia N. Natural frequency analysis of imperfect FG sandwich plates resting on Winkler-Pasternak foundation. *Materials Today: Proceedings*, 53(1), 153-160, 2022. https://doi.org/10.1016/j.matpr.2021.12.485.

[80]Civalek, Ö., Avcar, M. Free vibration and buckling analyses of CNT reinforced laminated non-rectangular plates by discrete singular convolution method. *Engineering with Computers*. 2020. https://doi.org/10.1007/s00366-020-01168-8

[81]Arslan E., Mack W., Apatay T. Thermo-mechanically loaded steel/aluminum functionally graded spherical containers and pressure vessels. *International Journal of Pressure Vessels and Piping*. 191, 104334, 2021. https://doi.org/10.1016/j.ijpvp.2021.104334

Critical Buckling Load of SiCNTs: A Molecular Dynamics Study on Gas Sensing

Kadir Mercan [a*], *Ömer Civalek* [b]

[a] Department of Civil Engineering, Faculty of Architecture-Engineering, Burdur Mehmet Akif Ersoy University
[b] Research Center for Interneural Computing University, China Medical University, Taichung, Taiwan
[*]E-mail address: kmercan@mehmetakif.edu.tr [a*], civalek@yahoo.com [b]

ORCID numbers of authors:
0000-0003-3657-6274[a], 0000-0003-1907-9479[b]*

Abstract

Silicon carbide nanotube (SiCNT) come forward in the great variety of nanotubes with higher durability until 1600 °C (in air) while carbon nanotube can stay stable until 600 °C (in air). First five buckling loads of single SiCNT placed between source and drain metal electrodes in nano sized field effect transistors (FET) is investigated using two different molecular dynamics methods. L.A.M.M.P.S. software and Gromacs package is used to perform molecular dynamics analyzes. Armchair structure of SiCNT with chiralities (10,0), (12, 0), (14, 0), (16, 0) were selected with 400, 480, 560, 640 atoms respectively. Results demonstrate clearly that longest nanotube perform lower stability as nanotubes becomes fragile with more atom numbers. Except from (10, 0) armchair SiCNT, first mode occurs at lowest load and rise as the number of mode arise.

Keywords: SiCNT, Field Effect Transistors, LAMMPS, Gromacs, MD Simulation.

1. Introduction

Fullerenes may be the first steps into nanomaterials which was emerged in the mid- 1980s. Krästschmer et al. [1] introduced the bulk production of fullerenes. Fullerene can be stated as an allotrope of carbon which consists of carbon atoms connected by both single and double bonds in shape of hollow sphere, ellipsoid, tube, or many other shapes. The interest in carbon nanomaterials remained limited as the potential were not fully understand. In 1991, with the discovery of carbon nanotube (CNT) by Iijima [2], carbon nanostructures gained wide interest all around the world due to superior mechanical properties. In 2008, Wu et al. [3] presented the potential of using silicon carbide nanotube (SiCNT) in gas sensors. It is presented that CO and HCN molecules can be absorbed to Si atoms on the wall of SiCNTs with binding energies as high as 0.70 eV and can attract finite charge from SiCNTs. The potential of sensitivity and accurate results in gas sensing using SiCNT pointed researchers to further researches. In 2011, Wang and Liew [4] presented the SiCNT performing as a highly sensitive gas chemical sensor for formaldehyde comparing to CNT. The interaction between HCOH and SiCNTs was presented using density functional theory (DFT). Apart from absorbing CO and HCN molecules on SiCNT Jia et al. [5, 6] investigated the SO_2 absorbing potential on (5, 5) zigzag SiCNT using DFT. Chemisorbing of SO_2 molecules to the Si–C bonds of SiCNTs with a result of generating different charge distribution, resulting in ihe breaking of some S–C bonds. Recently, Lin et al. [7] presented that phosphorus-doped SiCNT (P-SiCNT) perform better than classical SiCNT on sensing SO_2 molecules using DFT and MD simulation methods. In 2022, Singh [8] investigated sulfur-doped SiCNT for detecting liquefied petroleum gas at room temperature.

Composites of silicon based nanostructures with carbon based structures gained attention. Dzunda et al. [9] investigated the mechanical, physical properties and tribological behavior of four types of silicon carbide composites with addition of carbon nanotubes to enhance the electrical conductivity of nanotube. For two composites electrical conductivity reached values of 1448 S/m and 2873 S/m. Shen et al. [10] investigated the fatigue strengthening of carbon/carbon composites modified with carbon nanotubes and silicon carbide nanowires. Taguchi et al. [11] presented the synthesis of a novel hybrid carbon nanomaterials inside silicon carbide nanotubes using ion irradiation of a C-SiC coaxial nanotube with 200-keV Si ions at room temperature. Taguchi et al. accomplished to obtain one-dimensionally stacked graphene nanodisks with diameters less than 50 nm with cylindrical MWCNTs, inside an amorphous SiCNT. Tony et al. [12], using microwave heating, presented the synthesis of one-dimensional silicon carbide nanomaterial from the blend of SiO_2 particles with two types of CNTs. This work demonstrated that types of one dimensional SiCNWs (hollow or solid) can be selected using various types of CNTs together with proposing a high efficiency microwave heating method. Uzun [13] presented the production of reinforced aluminum foam using SiC particles and CNT together and separately. Powder metallurgy method was used to produce SiC particles and CNT reinforced aluminum foam. It is clearly demonstrated that addition of reinforcing affected the elastic–plastic deformation behavior. Yang et al. [14] presented the electromagnetic-shielding of CNT/graphene foam (GF)/SiC composites by in-situ growth of CNT in GF resulting in superior electromagnetic interface (EMI) shielding effectiveness (SE). Zhang et al. [15] developed a one-step method to synthesize Si/CNTs nanocomposite. A magnesium reduction process was developed using SiO_2 particles. Si/SiC/CNT nanocomposite were obtained for using in lithium ion batteries (LIBs) with a stable capacity of ~1100 mAh g^{-1} together with a capacity retention of about 83.8% at a current density of 100 mA g^{-1} after 200 cycles.

As setting up a new laboratory to perform nano sized analyzes can reach astronomical costs, researchers prefer to perform analyzes using classical mechanic [16-19] which leads to give non-accurate results, higher order continuum mechanics theories such as strain gradient [20-23], couple stress [21, 24-26], nonlocal elasticity [27-30], surface elasticity [31-35] etc. Furthermore, finite element [36, 37] and DSC method [38-43] methods were also used to perform analyzes without the need of a lab. On the other hand, modal and bending analyzes of nanostructures has been one of the most applied investigation on nanostructures [44-52].Theoretical works were promising in case of the ability to perform hundreds of analyzes in very short time [38, 53-61]. The most important disadvantage in theoretical works were the accuracy of methods used. It is not always possible to check the accuracy of method for each samples analyzed.

Molecular dynamics (MD) methods differ from other methods as researchers have the ability to model each atom separately. This ability leads to very accurate result with a usage of valid model. The interaction between both bonded and non-bonded atom is modeled in MD simulations. Another advantage of modeling each atom separately is to model imperfect nanostructures such as damaged structures or particular nanostuctures.

2. Silicon Carbide Nanotube (SiCNT)

Carbon based nanostructures such as graphene, fullerene, and CNTs has been the keystone of nanomaterials. First, with Young's modulus around 1000 GPa, CNTs attracted attention for a limited variety of potential using area with very high surface to volume ratio. After years, extraordinary electrical conductivity of CNT were introduced. Together with superior mechanical properties, electrical conductivity improved the interest to nanostructures drastically. Superior conductivity with very high durability made possible to use nanostuctures

in microelectromechanical (MEMS) and nanoelectromechanical systems (NEMS). Furthermore, the resistance to high-temperature of CNT and carbon based nanomaterials were limited. Due to the limited durability in high temperatures, scientists have developed a new structure of nanotube [62-64]. The structure consist of silicon (Si) atoms together with carbon atoms. Si atoms bonded to C atoms formed a novel structure in sheet form called silicon carbide sheet. Analyzes demonstrated that the durability under very-high temperatures were promising while the mechanical strength were not as high as fully carbon based structures. Silicon carbide nanotubes (SiCNTs) can be obtained by simply rolling silicon carbide sheets. SiCNT can keep stable until 1600 ºC (in air), whereas Carbon nanotubes were limited to stay stable until 600 ºC [65, 66]. Silicon based structures come forward with its strength to high temperature. In Fig. 1, the process of obtaining SiCNT from silicon carbide sheet is demonstrated. As it can be seen, the easiest way to obtain nanotube from nanosheet is to simply roll the flat structure until bonding.
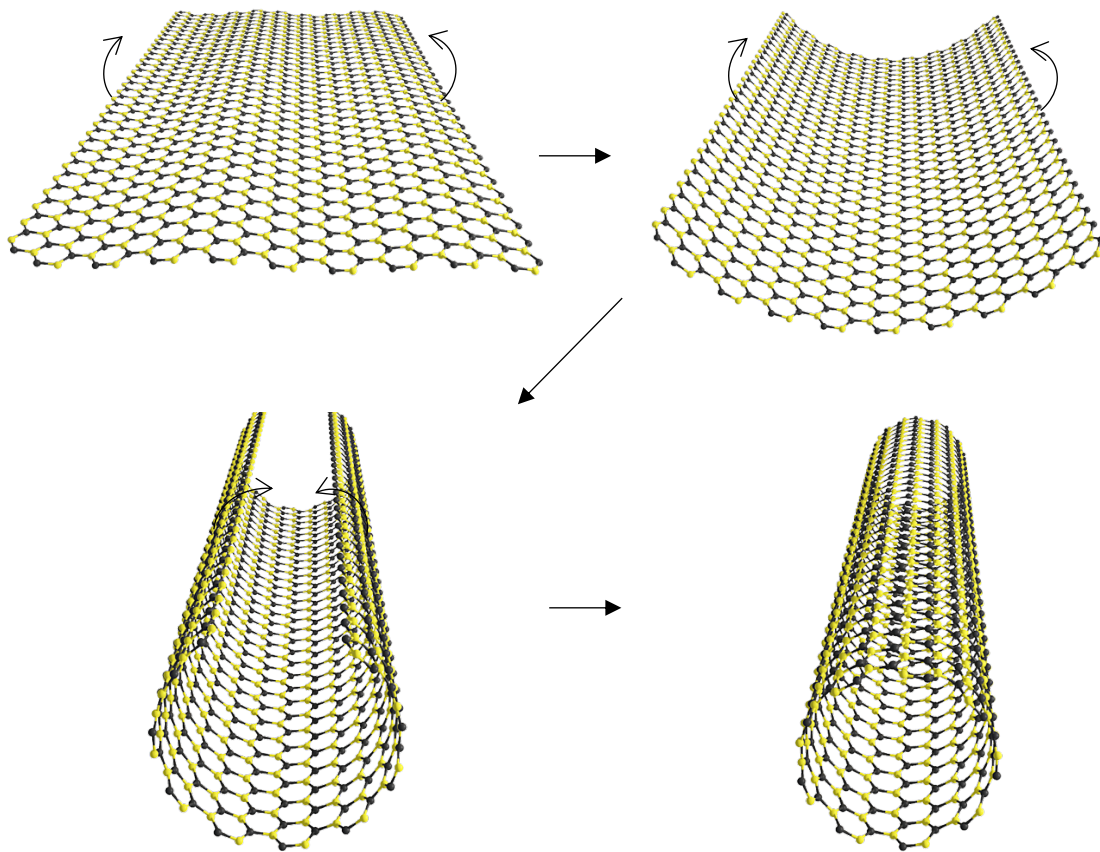

Fig. 1. Producing SiCNT from Silicon Carbide Sheet

Modeling nanotubes using continuum mechanic and MD simulation has great difference. As it can be clearly seen from bottom part of Fig. 2, the nanotube transform to cylindrical homogenous structure in continuum mechanic. This can lead to non-accurate results. On the other side, as it can be seen from the top part of Fig. 2, modeling each atoms separately in MD simulation would lead to more accurate results.
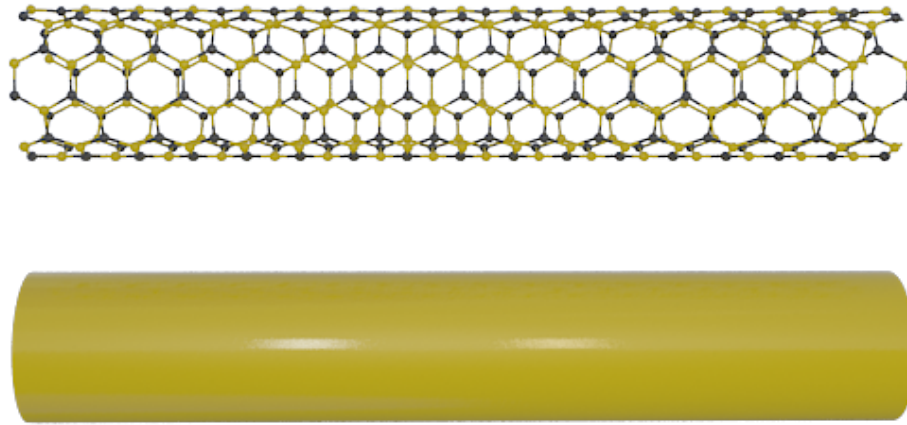
Fig. 2. Modeling SiCNT on MD simulation (top) and continuum mechanic (bottom)

Nanostructures can be presented using three main groups comparing bonding angles. The angle of nanostructures are rolled is represented by a pair of indices *(n,m)*. Here *'n and m'* denote the number of unit vectors along two directions in the hexagonal structures of silicon carbide sheet. As it can be seen in Fig. 3, if *m=0,* the structure is called *zigzag*, and if *n=m*, the structure is called *armchair*. In any other case, the structure will be called *chiral*. Armchair, zigzag, and chiral nanotubes have different physical, mechanical, and electrical properties which are neglected in continuum mechanic. In analyzes, SiCNTs with (10, 0), (12, 0), (14, 0), (16, 0) chirality of nanotubes are examined with following given stoichiometries in Table 1.

Table 1. Stoichiometries of SiCNTs

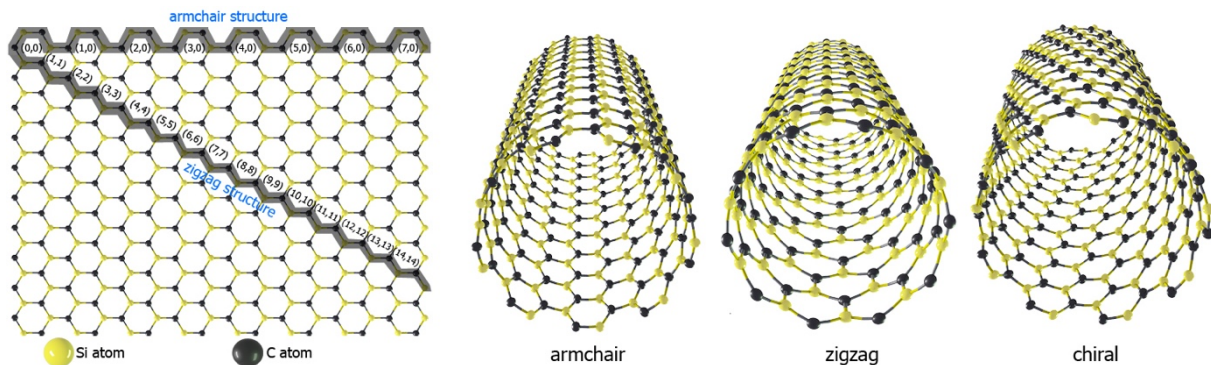| Chirality	Diameter (nm)	Numbers of atoms in sample
(10, 0)	0.9924	400
(12, 0)	1.1091	480
(14, 0)	1.3893	560
(16, 0)	1.5878	640

Fig. 3. Armchair, zigzag, and chiral SiCNT [65]

Silicon carbide nanostructures are widely used in gas sensors due to its durability under high temperature [67]. CO and HCN gases can be captivated on SiCNT at Si lattice sites in sensors. Any captivation on sensor leads to fluctuation in binding energy. Fluctuation in binding energy change the conductivity of SiCNT on sensor. Electro-transducers measures the absorbed gas molecules [68]. Field effect transistors (FET) is presented in Fig. 4. As it can be seen from Fig. 4 the nanotube take place between source and drain metal electrodes.
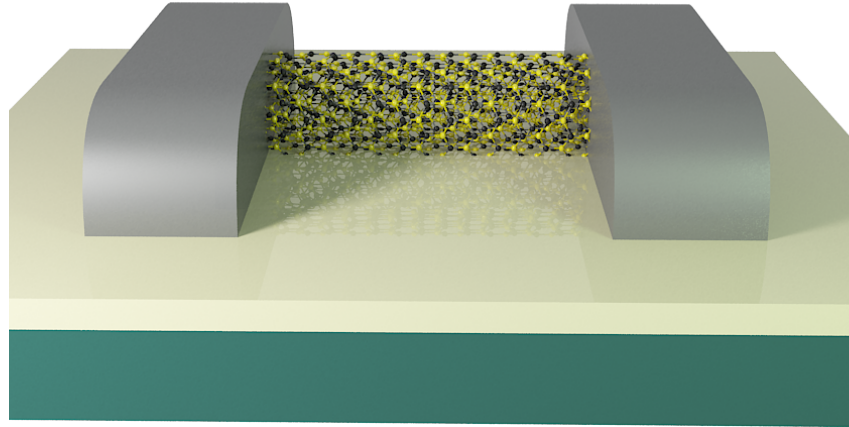

Fig. 4. SiCNT in NEMS

3. Large-Scale Atomic/Molecular Massively Parallel Simulator (LAMMPS)

Molecular dynamics (MD) method allows to examine the material properties and dynamic behavior of nanoscaled structures such as nanotubes, nanoplates etc. MD differ from other methods in case of the ability to calculate each samples material properties separately from the interactions between atoms. This create the opportunity to be able to analyze imperfect structures with more accurate results. The reactive empirical bond order potential (REBO) which was exposed by Brenner in 1990 can be accepted as the starting point of calculating potential between atoms of hydrocarbons including nonlocal effect [69]. REBO is based on Tersoff's covalent-bonding formalism and include extra terms for correcting overbinding. In our previous work, interatomical potentials calculations was expressed as follow [70]:

$$2E = \sum_i \quad \sum_{j \neq 1} f_c(r_{ij}) \ \left(f_T(r_{ij}) + b_{ij} f_E(r_{ij}) \right) \tag{1}$$

Where

$$f_T(r \ ) = A e^{(-\lambda_1 r)} \tag{2}$$

$$f_E(r \ ) = -B e^{(-\lambda_2 r)} \tag{3}$$

$$f_C(r\ ) = 0.5 - 0.5sin\left(\frac{\pi}{2}\left(\frac{r-D}{D}\right)\right) \quad \begin{matrix} 1 & : r < R - D \\ & : R - D < r < R + D \\ 0 & : r > R + D \end{matrix} \qquad (4)$$

$$b_{ij} = \sqrt[2n]{\frac{1}{1+\beta^n \xi_{ij}^n}} \qquad (5)$$

$$\xi_{ij} = \sum_{k \neq i,j} f_C(r_{ij}) g(\theta_{ijk}) e^{\lambda_3^m (r_{ij}-r_{ik})^m} \qquad (6)$$

$$g(\theta) = \gamma_{ijk}\left(1 + \frac{c^2}{d^2} - \frac{c^2}{d^2+(cos\theta - cos\theta_0)^2}\right) \qquad (7)$$

Where i,j and k represent the atom numbers, θ is the angle between atoms, r is the distance between Si and C atoms. Furthermore, f_T act in place of a two-body term, f_C represent cutoff term while f_E stand for three-body interactions.

4. Gromacs Package

Gromacs is a package which allow to perform molecular dynamics analyzes using interactions between neighboring atoms. Nanotubes were modeled subjected to compressive loading with different geometric parameters. To calculate the interactions between atoms, the force potentials from both bonding together with nonbonding interactions needs to be taken into consideration. Non-bonding interactions occurs due to van der Waals force instead of electrostatic interactions. Assorted potential functions can be used to obtain forces needed. In this paper Lennard-Jones potentials were used. The equation of motion to obtain the ith atoms force can be stated as

$$F_i = \sum_{\substack{j=1 \\ j \neq i}}^{N} \frac{\partial \emptyset_{ij}(r_{ij})}{\partial r_{ij}} \frac{r_j-(r_i)}{|r_j-(r_i)|} \qquad (8)$$

Whilst dynamical process, the location of calculated i^{th} atom were presented as $r_i(t)$ at specific time (t). Newton's second law were followed on the differ in atomic positions leading to capturing the fluctuation in the energy of the system. Small time steps were applied to capture the fluctuation as follows together with Verlet algorithm to reduce computational time

$$F_i = m_i \frac{\partial^2 r_i}{\partial t^2}, \quad i = 1,2,\dots,N \qquad (9)$$

4. Numerical Results

In this section the comparative buckling analysis of SiCNT using L.A.M.M.P.S and Gromacs package is presented. Armchair SiCNT structures with chiralities (10, 0), (12, 0), (14, 0), (16, 0) are examined. Calculated Young's modulus of SiCNTs with (10, 0), (12, 0), (14, 0), (16, 0) chirality varies from 508.3 GPa to 518.1 GPa.

a) (10, 0)

b) (12, 0)
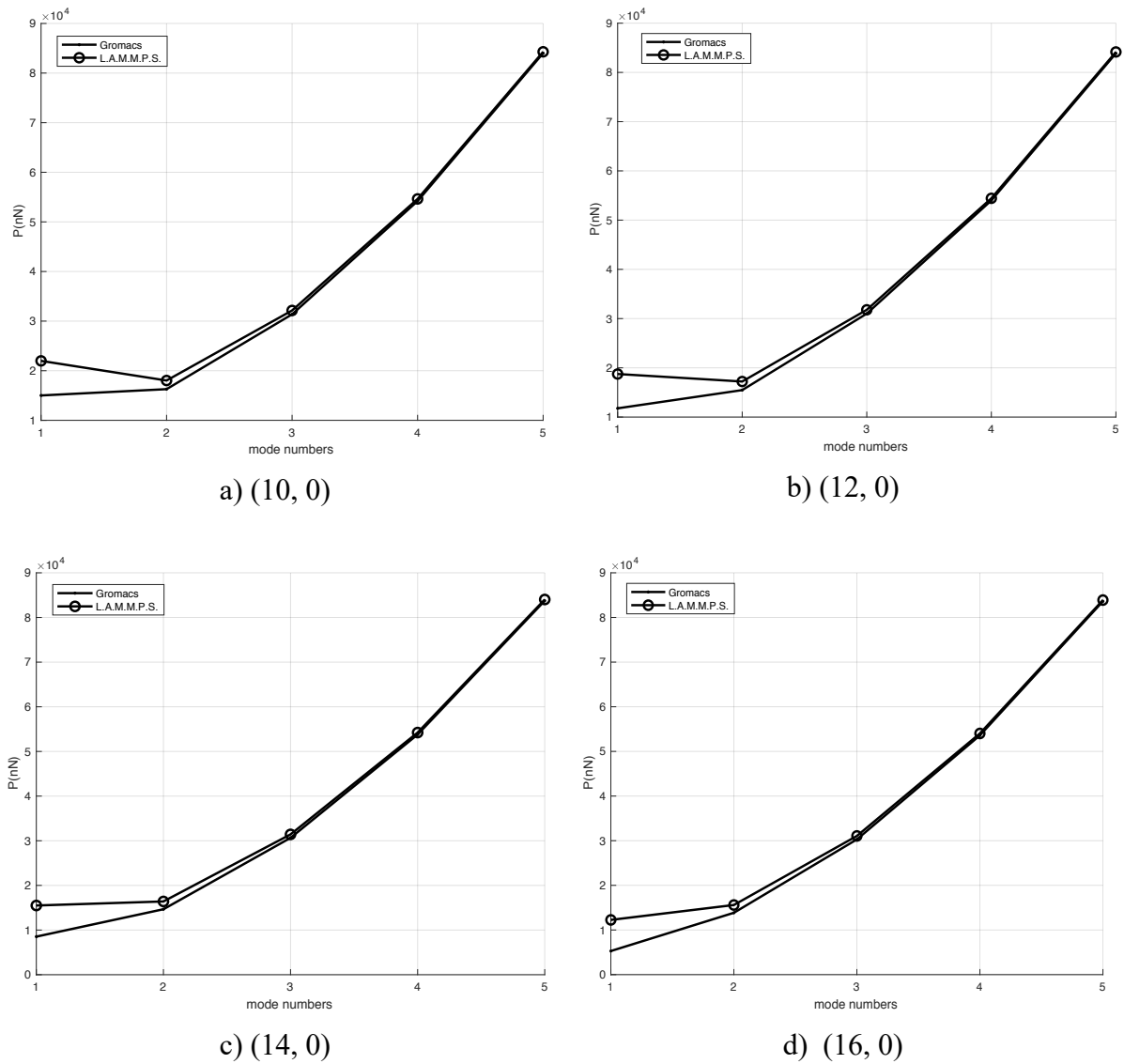

c) (14, 0)

d) (16, 0)

Fig. 5. First five modes of stability analysis

Armchair (16, 0) SiCNT with 640 atoms perform lowest stability comparing to other structures for both MD simulation results while (10, 0) with 400 atoms perform highest stability. L.A.M.M.P.S. analysis for (10, 0) armchair SiCNT results in lower second mode which means second mode shape occurs before first mode of buckling while Gromacs differ from L.A.M.M.P.S. in this analysis. Results are plotted for first five modes of (10,0), (12, 0), (14, 0), (16, 0) in Fig. 5 (a-d) respectively.

5. Conclusions

As biocompatible materials, SiC nanostructures have many applications in biomedicine. SiC is used in coatings on biomedical implants with excellent wear-resistant and non-hazardous to health, also SiC films with very small pores are used as semi-permeable biomaterials. Biomorphic SiC ceramics coated with bioactive glass show great promise as dental and orthopedic implants with improved mechanical and chemical properties. In current work

SiCNTs stability analysis is investigated using two different molecular dynamics packages. Results indicates that the size of nanotube effect the stability as nanotubes becomes fragile with more atom numbers. Except from (10, 0) armchair SiCNT, first mode occurs at lowest load and rise as the number of mode arise.

References

[1] Krätschmer, W., Lamb, L.D., Fostiropoulos, K., Huffman, D.R., Solid C60: a new form of carbon. *Nature*, 347(6291), 354-358, 1990.

[2] Iijima, S., Helical microtubules of graphitic carbon. *nature*, 354(6348), 56, 1991.

[3] Wu, R.Q., Yang, M., Lu, Y.H., Feng, Y.P., Huang, Z.G., Wu, Q.Y., Silicon Carbide Nanotubes As Potential Gas Sensors for CO and HCN Detection. *Journal of Physical Chemistry C*, 112(41), 15985-15988, 2008.

[4] Wang, X., Liew, K.M., Silicon Carbide Nanotubes Serving as a Highly Sensitive Gas Chemical Sensor for Formaldehyde. *Journal of Physical Chemistry C*, 115(21), 10388-10393, 2011.

[5] Jia, Y.B., Zhuang, G.L., Wang, J.G., Electric field induced silicon carbide nanotubes: a promising gas sensor for detecting SO2. *Journal of Physics D-Applied Physics*, 45(6), 2012.

[6] Wang, J.G., Chen, W.L., Jia, Y.B., Zhuang, G.L., Electric field induced silicon carbide nanotubes: A promising gas sensor for detecting SO2. *Abstracts of Papers of the American Chemical Society*, 244, 2012.

[7] Lin, W.Q., Li, F., Chen, G.H., Xiao, S.T., Wang, L.Y., Wang, Q., A study on the adsorptions of SO2 on pristine and phosphorus-doped silicon carbide nanotubes as potential gas sensors. *Ceramics International*, 46(16), 2020.

[8] Singh, R.S., Sulfur-doped silicon carbide nanotube as a sensor for detecting liquefied petroleum gas at room temperature. *Diamond and Related Materials*, 124, 2022.

[9] Dzunda, R., Fides, M., Hnatko, M., Hvizdos, P., Mudra, E., Medved, D., Kovalcikova, A., Milkovic, O., Mechanical, physical properties and tribological behaviour of silicon carbide composites with addition of carbon nanotubes. *International Journal of Refractory Metals & Hard Materials*, 81, 272-280, 2019.

[10] Shen, Q.L., Song, Q., Li, H.J., Xiao, C.X., Wang, T.Y., Lin, H.J., Li, W., Fatigue strengthening of carbon/carbon composites modified with carbon nanotubes and silicon carbide nanowires. *International Journal of Fatigue*, 124, 411-421, 2019.

[11] Taguchi, T., Yamamoto, S., Ohba, H., Synthesis of novel hybrid carbon nanomaterials inside silicon carbide nanotubes by ion irradiation. *Acta Materialia*, 173, 153-162, 2019.

[12] Tony, V.C.S., Voon, C.H., Lim, B.Y., Al-Douri, Y., Gopinath, S.C.B., Arshad, M.K.M., Ten, S.T., Parmin, N.A., Ruslinda, A.R., Synthesis of silicon carbide nanomaterials by microwave heating: Effect of types of carbon nanotubes. *Solid State Sciences*, 98, 2019.

[13] Uzun, A., Production of aluminium foams reinforced with silicon carbide and carbon nanotubes prepared by powder metallurgy method. *Composites Part B-Engineering*, 172, 206-217, 2019.

[14] Yang, Y.L., Zuo, Y., Feng, L., Hou, X.J., Suo, G.Q., Ye, X.H., Zhang, L., Powerful and lightweight electromagnetic-shielding carbon nanotube/graphene foam/silicon carbide composites. *Materials Letters*, 256, 2019.

[15] Zhang, Y., Hu, K., Zhou, Y.L., Xia, Y.B., Yu, N.F., Wu, G.L., Zhu, Y.S., Wu, Y.P., Huang, H.B., A Facile, One-Step Synthesis of Silicon/Silicon Carbide/Carbon Nanotube Nanocomposite as a Cycling-Stable Anode for Lithium Ion Batteries. *Nanomaterials*, 9(11), 2019.

[16] Wang, Y., Wang, X.X., Ni, X.G., Wu, H.A., Buckling behavior of carbon nanotube under compression. *Acta Physica Sinica*, 52(12), 3120-3124, 2003.

[17] Wang, C.Y., Ru, C.Q., Mioduchowski, A., Elastic buckling of multiwall carbon nanotubes under high pressure. *Journal of Nanoscience and Nanotechnology*, 3(1-2), 199-208, 2003.

[18] Li, C., Guo, W.L., Continuum mechanics simulation of post-buckling of single-walled nanotubes. *International Journal of Nonlinear Sciences and Numerical Simulation*, 4(4), 387-393, 2003.

[19] Akgöz, B., Mercan, K., Demir, Ç., Civalek, Ö., Static analysis of beams on elastic foundation by the method of discrete singular convolution. *International Journal of Engineering and Applied Sciences*, 8(3), 67-73, 2016.

[20] Fleck, N., Hutchinson, J., Strain gradient plasticity. *Advances in applied mechanics*, 33, 296-361, 1997.

[21] Yang, F., Chong, A., Lam, D.C., Tong, P., Couple stress based strain gradient theory for elasticity. *International Journal of Solids and Structures*, 39(10), 2731-2743, 2002.

[22] Arda, M., Evaluation of optimum length scale parameters in longitudinal wave propagation on nonlocal strain gradient carbon nanotubes by lattice dynamics. *Mechanics Based Design of Structures and Machines*, 1-24, 2020.

[23] Arda, M., Buckling Analysis of Intermediately Supported Nanobeams via Strain Gradient Elasticity Theory. *International Journal of Engineering and Applied Sciences*, 12(4), 163-172, 2022.

[24] Ma, H., Gao, X.-L., Reddy, J., A microstructure-dependent Timoshenko beam model based on a modified couple stress theory. *Journal of the Mechanics and Physics of Solids*, 56(12), 3379-3391, 2008.

[25] Reddy, J., Microstructure-dependent couple stress theories of functionally graded beams. *Journal of the Mechanics and Physics of Solids*, 59(11), 2382-2399, 2011.

[26] Zhou, S., Li, Z., Length scales in the static and dynamic torsion of a circular cylindrical micro-bar. 2001.

[27] Eringen, A.C., On differential equations of nonlocal elasticity and solutions of screw dislocation and surface waves. *Journal of applied physics*, 54(9), 4703-4710, 1983.

[28] Eringen, A.C., *Nonlocal continuum field theories*2002; Springer Science & Business Media,2002.

[29] Arda, M., Axial dynamics of functionally graded Rayleigh-Bishop nanorods. *Microsystem Technologies-Micro-and Nanosystems-Information Storage and Processing Systems*, 27(1), 269-282, 2021.

[30] Arda, M., Kısmi yayılı yük etkisindeki nano kirişlerin dinamik analizi. *Mühendislik Bilimleri ve Tasarım Dergisi*, 8(2), 417-428, 2022.

[31] Dingreville, R., Qu, J., Cherkaoui, M., Surface free energy and its effect on the elastic behavior of nano-sized particles, wires and films. *Journal of the Mechanics and Physics of Solids*, 53(8), 1827-1854, 2005.

[32] Mercan, K., Civalek, Ö., Buckling Analysis of Silicon Carbide Nanotubes (SiCNTs). *International Journal of Engineering & Applied Sciences (IJEAS)*, 8(2), 101-108, 2016.

[33] Rahmani, O., Asemani, S., Hosseini, S., Study the surface effect on the buckling of nanowires embedded in Winkler–Pasternak elastic medium based on a nonlocal theory. *Journal of Nanostructures*, 6(1), 90-95, 2016.

[34] Sharma, P., Ganti, S., Size-dependent Eshelby's tensor for embedded nano-inclusions incorporating surface/interface energies. *Journal of Applied Mechanics*, 71(5), 663-671, 2004.

[35] Sharma, P., Ganti, S., Bhate, N., Effect of surfaces on the size-dependent elastic state of nano-inhomogeneities. *Applied Physics Letters*, 82(4), 535-537, 2003.

[36] Numanoglu, H.M., Mercan, K., Civalek, O., Finite element model and size-dependent stability analysis of boron nitride and silicon carbide nanowires/nanotubes. *Scientia Iranica*, 26(4), 2079-2099, 2019.

[37] Mercan, K., Civalek, Ö., Modal Analysis of Micro and Nanowires Using Finite Element Softwares. *International Journal of Engineering and Applied Sciences*, 10(4), 291-304, 2018.

[38] Civalek, Ö., Kiracioglu, O., Free vibration analysis of Timoshenko beams by DSC method. *International Journal for Numerical Methods in Biomedical Engineering*, 26(12), 1890-1898, 2010.

[39] Demir, C., Mercan, K., Civalek, O., Determination of critical buckling loads of isotropic, FGM and laminated truncated conical panel. *Composites Part B-Engineering*, 94, 1-10, 2016.

[40] Ersoy, H., Mercan, K., Civalek, O., Frequencies of FGM shells and annular plates by the methods of discrete singular convolution and differential quadrature methods. *Composite Structures*, 183, 7-20, 2018.

[41] Mercan, K., Baltacioglu, A.K., Civalek, O., Free vibration of laminated and FGM/CNT composites annular thick plates with shear deformation by discrete singular convolution method. *Composite Structures*, 186, 139-153, 2018.

[42] Mercan, K., Ebrahimi, F., Civalek, O., Vibration of angle-ply laminated composite circular and annular plates. *Steel and Composite Structures*, 34(1), 141-154, 2020.

[43] Mercan, K., Demir, Ç., Civalek, Ö., Vibration analysis of FG cylindrical shells with power-law index using discrete singular convolution technique. *Curved and Layered Structures*, 3(1), 2016.

[44] Hadji, L., Avcar, M., Civalek, Ö., An analytical solution for the free vibration of FG nanoplates. *Journal of the Brazilian Society of Mechanical Sciences and Engineering*, 43(9), 418, 2021.

[45] Civalek, O., Avcar, M., Free vibration and buckling analyses of CNT reinforced laminated non-rectangular plates by discrete singular convolution method. *Engineering with Computers*, 2020.

[46] Avcar, M., Hadji, L., Civalek, Ö., Natural frequency analysis of sigmoid functionally graded sandwich beams in the framework of high order shear deformation theory. *Composite Structures*, 276, 114564, 2021.

[47] Hadji, L., Avcar, M., Nonlocal free vibration analysis of porous FG nanobeams using hyperbolic shear deformation beam theory. *Advances in Nano Research*, 10(3), 281-293, 2021.

[48] Arda, M., Torsional Vibration Analysis of Carbon Nanotubes Using Maxwell and Kelvin-Voigt Type Viscoelastic Material Models. *European Mechanical Science*, 4(3), 90-95, 2022.

[49] Civalek, Ö., Baltacıoglu, A.K., Free vibration analysis of laminated and FGM composite annular sector plates. *Composites Part B: Engineering*, 157, 182-194, 2019.

[50] Civalek, Ö., Geometrically nonlinear dynamic and static analysis of shallow spherical shell resting on two-parameters elastic foundations. *International Journal of Pressure Vessels and Piping*, 113, 1-9, 2014.

[51] Akgöz, B., Civalek, Ö., Vibrational characteristics of embedded microbeams lying on a two-parameter elastic foundation in thermal environment. *Composites Part B: Engineering*, 150, 68-77, 2018.

[52] Demir, C., Mercan, K., Numanoglu, H.M., Civalek, O., Bending Response of Nanobeams Resting on Elastic Foundation. *Journal of Applied and Computational Mechanics*, 4(2), 105-114, 2018.

[53] Mercan, K., Işık, Ç., Akgöz, B., Civalek, O., Coordinate Transformation for Sector and Annular Sector Shaped Graphene Sheets on Silicone Matrix. *International Journal of Engineering & Applied Sciences (IJEAS)*, 7(2), 56-73, 2015.

[54] Mercan, K., Demir, Ç., Ersoy, H., Civalek, Ö., The effects of thickness on frequency values for rotating circular shells. *International Journal of Engineering & Applied Sciences (IJEAS)*, 8(1), 26-37, 2016.

[55] Mercan, K., Ersoy, H., Civalek, O., Free Vibration of Annular Plates by Discrete Singular Convolution and Differential Quadrature Methods. *Journal of Applied and Computational Mechanics*, 2(3), 128-133, 2016.

[56] Civalek, Ö., Free vibration of carbon nanotubes reinforced (CNTR) and functionally graded shells and plates based on FSDT via discrete singular convolution method. *Composites Part B: Engineering*, 111, 45-59, 2017.

[57] Demir, Ç., Akgöz, B., Erdinç, M.C., Mercan, K., Civalek, Ö., Elastik bir ortamdaki grafen tabakanın titreşim hesabı. *Gazi Üniversitesi Mühendislik-Mimarlık Fakültesi Dergisi*, 32(2), 2017.

[58] Demir, C., Akgoz, B., Erdinc, M.C., Mercan, K., Civalek, O., Free vibration analysis of graphene sheets on elastic matrix. *Journal of the Faculty of Engineering and Architecture of Gazi University*, 32(2), 551-562, 2017.

[59] Mercan, K., Akgöz, B., Demir, Ç., Civalek, Ö., Frequencies Values of Orthotropic Composite Circular and Annular Plates. *International Journal Of Engineering & Applied Sciences*, 9(2), 55-65, 2017.

[60] Numanoglu, H.M., Mercan, K., Civalek, Ö., Frequency and Mode Shapes of Au Nanowires Using the Continuous Beam Models. *International Journal of Engineering & Applied Sciences (IJEAS)*, 9(1), 55-61, 2017.

[61] Ersoy, H., Mercan, K., Civalek, Ö., Frequencies of FGM shells and annular plates by the methods of discrete singular convolution and differential quadrature methods. *Composite Structures*, 183, 7-20, 2018.

[62] Shimizu, T., Ishikawa, Y., Kusunoki, M., Nagano, T., Shibata, N., Creation of highly oriented freestanding carbon nanotube film by sublimating decomposition of silicon carbide film. *Japanese Journal of Applied Physics Part 2-Letters*, 39(10b), L1057-L1059, 2000.

[63] Kusunoki, M., Rokkaku, M., Suzuki, T., Epitaxial carbon nanotube film self-organized by sublimation decomposition of silicon carbide. *Applied Physics Letters*, 71(18), 2620-2622, 1997.

[64] Kusunoki, M., Suzuki, T., Kaneko, K., Ito, M., Formation of self-aligned carbon nanotube films by surface decomposition of silicon carbide. *Philosophical Magazine Letters*, 79(4), 153-161, 1999.

[65] Mercan, K., Numanoglu, H.M., Akgöz, B., Demir, C., Civalek, Ö., Higher-order continuum theories for buckling response of silicon carbide nanowires (SiCNWs) on elastic matrix. *Archive of Applied Mechanics*, 87(11), 1797-1814, 2017.

[66] Fan, J.-Y., Chu, P.K.-H., *Separate SiC Nanoparticles*, in *Silicon Carbide Nanostructures: Fabrication, Structure, and Properties*, J. Fan and P.K. Chu, Editors. 2014, Springer International Publishing; Cham, 131-193,2014.

[67] Wu, R., Yang, M., Lu, Y., Feng, Y., Huang, Z., Wu, Q., Silicon carbide nanotubes as potential gas sensors for CO and HCN detection. *The Journal of Physical Chemistry C*, 112(41), 15985-15988, 2008.

[68] Huang, J., Wan, Q., Gas sensors based on semiconducting metal oxide one-dimensional nanostructures. *Sensors*, 9(12), 9903-9924, 2009.

[69] Brenner, D.W., Empirical potential for hydrocarbons for use in simulating the chemical vapor deposition of diamond films. *Physical Review B*, 42(15), 9458-9471, 1990.

[70] Mercan, K., Civalek, O., Comparative Stability Analysis of Boron Nitride Nanotube using MD Simulation and Nonlocal Elasticity Theory. *International Journal of Engineering and Applied Sciences*, 13(4), 189-200, 2022.